FEDERAL UNIVERSITY OF PERNAMBUCO
TECHNOLOGY AND GEOSCIENCES CENTER
DEPARTMENT OF ELECTRONICS AND SYSTEMS
GRADUATE PROGRAM IN ELECTRICAL ENGINEERING

THALES HENRIQUE CASTRO DE BARROS

D-SHAPED OPTICAL FIBER SENSORS FOR THE OIL AND GAS INDUSTRY

Recife
2023

THALES HENRIQUE CASTRO DE BARROS

D-SHAPED OPTICAL FIBER SENSORS FOR THE OIL AND GAS INDUSTRY

Dissertation presented to the Graduate Program in Electrical Engineering at the Federal University of Pernambuco, as a partial requirement for obtaining the Master's degree in Electrical Engineering.

Concentration Area: Photonics.

Advisor: Prof. Dr. Joaquim Ferreira Martins Filho.

Recife

2023

Catalogação na fonte:
Bibliotecário Carlos Moura, CRB-4/1502

B277d Barros, Thales Henrique Castro de.
D-shaped optical fiber sensors for the oil and gas industry. / Thales Henrique Castro de Barros. – 2023.
74 f.: il.

Orientador: Prof. Dr. Joaquim Ferreira Martins Filho.
Dissertação (mestrado) – Universidade Federal de Pernambuco. CTG. Programa de Pós-Graduação em Engenharia Elétrica. Recife, 2023.
Inclui referências e apêndice.

1. Engenharia elétrica. 2. Fibra óptica com perfil-D. 3. Sensor de índice de refração. 4. Indústria de óleo e gás. 5. Fotônica. I. Martins Filho, Joaquim Ferreira (orientador). II. Título.

621.3 CDD (22. ed.)

UFPE
BCTG/2023-214

THALES HENRIQUE CASTRO DE BARROS

D-SHAPED OPTICAL FIBER SENSORS FOR THE OIL AND GAS INDUSTRY

Dissertation presented to the Graduate Program in Electrical Engineering at Technology and Geosciences Center of the Federal University of Pernambuco, as a partial requirement for obtaining the Master's degree in Electrical Engineering.

Concentration Area: Photonics.

Approved in: 28/08/2023.

EXAMINATION COMMITTEE

_____

Prof. Dr. Joaquim Ferreira Martins Filho (Advisor)
Federal University of Pernambuco

_____

Prof. Dr. Renato Evangelista de Araujo (Internal Examiner)
Federal University of Pernambuco

_____

Prof. Dr. Walter Margulis (External Examiner)
Pontifical Catholic University of Rio de Janeiro

I dedicate this work to all those who helped me on this journey because the fruits of my work today are the result of the seeds planted by each one of you.

To my mother, my biggest supporter and strength, Roseane.

To my father, Marcelo, my eternal source of advice and teaching.

To my grandmother, Cenira, for all the care that even today allows me to go through my moments of fragility.

To my Bruna, for all the love, care and affection that allow me to try to fly higher.

I also dedicate this work to the memory of the two fathers that life gave me and so soon left me: Cícero Pereira de Castro and Cícero Pereira de Castro Júnior. The life you lived inspires me and I hope one day I can look back proudly on honoring that legacy.

ACKNOWLEDGMENTS

To God for being my fortress, the light that illuminates my steps and who in his infinite mercy surrounded me with good people.

To my advisor, Professor Joaquim Ferreira Martins Filho, who, by receiving me while I was just a student with the desire to learn a little more, allowed me to follow the path I always dreamed of walking, changing my life.

To my co-advisor, Professor Henrique Patriota Alves, for all the support, especially in the last-minute revisions, for rooting for my success and supporting me in my failures

To my mother, Roseane do Nascimento de Castro, for all the affection, care, dedication and affection, responsible for keeping me walking in pursuit of my goals.

To my father, Marcelo Ricardo Carneiro de Barros, for all the support and advice that many times rescued me from my moments of doubt.

To my grandmother, Cenira Francisca de Castro, for being my maternal lap, my foster mother, my emotional support and my source of laughter.

To my partner and best friend, my dear Bruna Brito Liberal, for her silly humor, care and dedication. For helping me fight my insecurities and for vibrating with me in my achievements.

To all my family, especially my little ones, Kauã Henrique de Castro Santos and Giullia Rafaella de Castro Santos, for filling my life with happy moments.

To my late uncle, Cícero Pereira de Castro Júnior, for encouraging me to always aspire for knowledge, making it a tool to help others. His teachings shaped my actions, but his legacy shapes my life.

To my late grandfather, Cícero Pereira de Castro, for all the cheering, vibrancy and affection he showed in life for my achievements. Being able to take this step further without seeing you by my side hurts me with all my heart. Watch over me wherever you are.

To Auxiliadora Brito, Bismarck Lopes and Luma Liberal, angels that God placed in my life, to whom I owe for their affection, care and happy moments.

I also would like to thank the friends I made when joining the Optical Sensors Group, in particular Marianne Peixoto, Leonardo Miranda, Hebio Oliveira and Allamys Allan for all the precious teachings and, mainly, for the motivation.

Finally, I would like to thank the Human Resources Program 38.1 of the Brazilian National Petroleum Agency (PRH 38.1-ANP) for funding my research and financial support.

My walk is definitely better with you.

If I have seen further, it is by standing on the shoulders of giants.

– Sir Isaac Newton (Letter to Robert Hooke, 1965)

ABSTRACT

This study addresses the development of sensor devices based on D-shaped optical fibers, applying them as solutions to different problems faced by the oil and gas industry. The processes used in the fabrication and characterization of the devices are presented, as well as the results obtained from the construction of a computational model. A brief discussion on the divergences found between the numerical model and the experimental results is also presented, focusing on the effect of surface roughness of the D-shaped on the device response. Two different optical fiber technologies were used: plastic optical fibers (POF) and single-mode optical fibers (SMF). The particularities related to each type of optical fiber are also described, as well as the operating parameters of each of the devices produced, such as sensitivity and resolution. Various scenarios were explored, such as adulteration of fuels, detection of leaks in pipelines, level control and management of fertilizer use. From the point of view of adulteration, the sensors were used in tests involving the adulteration of diesel with kerosene, ethanol with water and gasoline with ethanol, encompassing a wide spectrum of possibilities, demonstrating the versatility of the sensor. In the context of leak detection, serial sensors spatially located through the use of optical time domain reflectometry were used. The results obtained showed a high sensitivity for detecting materials with a high refractive index, making the solution especially viable for detecting oil leaks in pipelines. Finally, the use of the sensor in fertilizer management was approached from a computational point of view, where the influence of geometric parameters on the response of the devices was also explored. The obtained results showed that sensors based on D-shaped optical fibers have great potential for the proposed applications, although they have been little explored in the literature.

Keywords: D-shaped optical fiber; refractive index sensor; oil and gas industry; photonics.

RESUMO

O presente trabalho aborda o desenvolvimento de dispositivos sensores à base de fibras ópticas com perfil D, aplicando-os como soluções para diferentes problemas enfrentados pela indústria de óleo e gás. São apresentados os processos utilizados na fabricação e caracterização dos dispositivos, bem como os resultados obtidos a partir da construção de um modelo computacional. Uma breve discussão sobre as divergências encontradas entre o modelo numérico e os resultados experimentais também é apresentada, com enfoque no efeito da rugosidade da superfície do perfil D sobre a resposta do dispositivo. Foram utilizadas duas tecnologias diferentes de fibras ópticas: as fibras ópticas plásticas (POF) e as fibras ópticas monomodo (SMF). As particularidades relacionadas a cada tipo de fibra óptica também são descritas, bem como os parâmetros operacionais de cada um dos dispositivos produzidos como a sensibilidade e a resolução. Foram explorados cenários diversos como a adulteração de combustíveis, a detecção de vazamentos em dutos, o controle de nível e o gerenciamento do uso de fertilizantes. Do ponto de vista da adulteração, os sensores foram utilizados em testes envolvendo a adulteração do diesel com querosene, do etanol com água e da gasolina com etanol, englobando um amplo espectro de possibilidades, demonstrando a versatilidade do sensor. No contexto da detecção de vazamentos, foram utilizados sensores em série espacialmente localizados através do emprego de reflectometria óptica no domínio do tempo. Os resultados obtidos mostraram uma alta sensibilidade para detecções de materiais com alto índice de refração, tornando a solução especialmente viável para detecção de vazamentos de óleo em dutos. Por fim, a utilização do sensor no gerenciamento de fertilizantes foi abordada do ponto de vista computacional, onde também foi explorada a influência dos parâmetros geométricos na resposta dos dispositivos. Os resultados obtidos mostraram que os sensores baseados em fibras ópticas com perfil D têm grande potencial para as aplicações propostas, embora tenham sido pouco exploradas na literatura.

Palavras-chave: fibra óptica com perfil-D; sensor de índice de refração; indústria de óleo e gás; fotônica.

LIST OF FIGURES

LIST OF TABLES

SUMMARY

1 INTRODUCTION

The oil and gas industry are currently undergoing a significant transformation driven by the global energy transition and the emergence of Industry 4.0. As the world seeks to transition to cleaner and more sustainable energy sources, the traditional oil and gas industry faces increasing challenges to adapt and remain competitive in this evolving landscape. This transition requires a shift towards greener practices, greater efficiency and greater operational reliability. In this context, solutions based on optical fiber sensors have become popular due to their operational characteristics, being used mainly in sensing, contributing to increase the reliability and efficiency of the process, in addition to resulting in the reduction of risks and the mitigation of environmental damage.

1.1. MOTIVATION AND CONTEXTUALIZATON

In recent years, optical fiber-based devices have gained significant attention and popularity worldwide. This surge in interest can be attributed to the central role that optical fiber technology plays in modern telecommunications networks. With its high bandwidth, low latency, and electromagnetic immunity, optical fibers have not only swiftly replaced traditional metallic cable-based telecommunication networks, but has also facilitated the development of critical technologies for the fourth industrial revolution, as the Internet of Things (IoT). Still yes, it is worth mentioning that while the IoT have the potential to enhance wireless connections, this approach is primarily applicable to the final stages of the network. From there, optical networks remain the most effective solution for the backbone composition because they provide reliable and efficient communication across long distances and high data volumes.

Another important point is the emergence of a hyperconnected structure due to the expansion in the number of connected devices supported by the IoT and other concepts like smart cities and mobile networks with higher frequencies and shorter ranges. This structure provides an increase in the demand and diffusion of optical fibers networks, solidifying their significance in supporting the evolving technological landscape. Finally, the creation of these hyperconnected environments full of intelligent devices integrated by optical networks also is a favorable ecosystem for the development of a specific group of optical devices: optical fiber sensors.

Optical fiber sensors also benefit from the same characteristics that have placed optical fiber at the foundation of all modern telecommunications. The high bandwidth, for example, allows arrangements in which a given optical signal can be used to amplify a second signal that normally would not be detected, allowing temperature measurement through Raman scattering. The low optical loss together with the ability for multiple signals to be transmitted simultaneously in the same optical fiber are also differentials, as they allow extensive sensor networks or the pre-existing infrastructure for communication can also be used for sensing purposes.

In general, these characteristics have contributed to the popularization of optical sensors in several industrial sectors, however, specifically in the context of the oil and gas industry, two other characteristics have been fundamental for the use of these devices: a high degree of passivity and reliability. These characteristics are valued because it is not uncommon for processes within this industry that use large electrical machines or that occur under adverse conditions, such as in the presence of corrosive, explosive atmospheres or immersed in water. This scenario means that traditional sensors are taken close to their limit conditions and that they need a large technological investment to allow their operation without major problems. On the other hand, optical fiber naturally does not suffer electromagnetic interference, does not generate sparks or heat, has high thermochemical resistance and can operate completely submerged, justifying the efforts for its implementation.

Complementarily, the oil and gas industry face a challenging scenario, although it still ranks as one of the largest industries in the world. In view of the progress of the energy transition process promoted by climate change, a progressive replacement of petroleum-derived fuels by other more sustainable energy sources is expected. This process could potentially put an end to all industrial activities aimed at extracting and refining oil, affecting a billionaire market. To overcome these problems, investments have been made to mitigate the impacts of this industry and increase the efficiency of its processes. Within this context and in view of all the characteristics already presented of optical fibers, optical sensors can be key solutions in the strategy adopted by this industry during this transition period.

1.2. OBJECTIVES

The objectives outlined during the development of this work are listed below. Initially, the general objective of the project will be shown, followed by the specific objectives.

1.2.1 General Objective

Develop refractive index sensors based on the interaction between the evanescent wave and the sensed medium through the use of the device known as D-shaped optical fiber and apply them to the context of the oil and gas industry.

1.2.2 Specific Objectives

a) Study the production processes used by the oil and gas industry;
b) Study the main strategies used in fuel adulteration;
c) Identify the state of the art of optical fiber sensors applied in the oil and gas industry;
d) Adjust and develop the instrumentation used in the sensor fabrication process;
e) Fabricate single-mode D-shaped optical fiber;
f) Fabricate plastic D-shaped optical fiber;
g) Characterize each sensor produced;
h) Determine the refractive index value of different fuel samples.

1.3. WORK ORGANIZATION

The present work is subdivided in eight different chapters. At the end, bibliographical references are also listed.

Chapter 2: It contains the necessary theoretical review of the concepts covered in the course of the other chapters and in the execution of the project. A brief explanation is given about the current context of the oil and gas industry, the challenges faced by this sector and how optical fiber sensors are inserted in this context. Also discussed are the fundamentals behind the operation of optical fiber and the structure known as D-shaped, used as the basis for the proposed device.

Chapter 3: It contains a description of the instrumentation and methodology used during the fabrication, characterization and execution of measurements using D-shaped optical fibers. It also presents the numerical parameters used in the construction of the presented computational model, through COMSOL Multiphysics.

Chapter 4: Displays the first group of results obtained: numerical results. Based on these results, it establishes the expected standard behavior for D-shaped optical fiber, indicating

different operating ranges, in addition to evaluating possible differences between the responses obtained from the modeling of the different types of optical fiber used.

Chapter 5: It presents the results obtained through the use of the proposed sensors as fuel adulteration detectors. Three different adulteration scenarios are investigated: ethanol adulteration with the addition of water, gasoline adulteration using ethanol and the addition of kerosene to diesel. In each case, the operating parameters of the devices, such as sensitivity and resolution, are presented.

Chapter 6: It presents the results obtained from the construction of a device capable of spatially detecting and locating oil leaks in pipelines. Such a device is composed of D-shaped optical fibers in series and uses a commercial Optical Time Domain Reflectometer (OTDR) for this location. Scenarios are evaluated with sensor elements submerged in water and oil, in addition to atmospheric air, and the response in each case is also presented.

Chapter 7: It presents the exploration of the computational model built initially for characterization, applying it in the detection of sulfate and nitrate ions by absorptiometry. Due to the participation of these ionic species in the absorption of nutrients by plants, this detection is used in order to propose a device that can be used in managing the use of fertilizers. It also presents the influence of geometric parameters on the device's response, serving as a basis for improvements in the fabrication process.

Chapter 8: It exposes the final considerations, highlighting the main contributions obtained with the execution of this Dissertation and the future perspectives for the next works.

2 THEORETICAL FOUNDATION

This chapter aims to present the current context in which this work is inserted. Firstly, in Section 2.1, a general context of the Oil and Gas Industry and challenges in the management of pipelines or the optimization of fertilizer application was presented. After that, the discussion is focused on the current state of the art of optical fiber sensors for oil and gas applications. This discussion is based on a bibliometric analysis and is presented in Section 2.2. Lastly, the functioning of the optical fiber and the phenomenon of the evanescent wave are presented in Section 2.3. These topics are fundamentals for the introduction of the D-shaped optical fibers, the theme of this work and presented in Section 2.4.

2.1. THE CURRENT CONTEXT OF THE OIL AND GAS INDUSTRY

The oil and gas sector currently faces a challenging scenario, as society has become increasingly concerned about the environmental impacts of its activities. This paradigm shift becomes more evident when we assess the perspectives of the sector at the beginning of the 21st century, a period associated with the beginning of the intensification of the environmental agenda. Around the 2000s, reports pointed out that the biggest problem in the sector was the gap between demand growth and the availability of extractable reserves (Longwell, 2002). This discussion restricted any environmental concern to the maintenance of wells and production levels, in addition to associating the green agenda with retrogression, as environmentalists sought to hinder activities in areas that were especially sensitive to environmental degradation, such as the province of Alaska (Longwell, 2002).

In the last decade, the discourse about the future of the oil and gas industry has given way to discussions about the environmental impacts of the sector's activities (Finley, 2012). In view of this, reports from the beginning of the last decade began to point out the progressive loss of the market for alternative technologies such as biofuels and other sustainable energy sources (Finley, 2012; Zou et al., 2016). This competition should not necessarily imply a reduction in production levels, bearing in mind that global energy consumption is growing at an accelerated pace and the sector continuously invests, aiming at increasing the efficiency and reliability of its operations (Zou et al., 2016). Even so, with these discussions, expectations change from a scenario of absolute optimism to consolidating the idea that oil and gas production should reach its peak and then enter into progressive decline in the coming decades (Zou et al., 2016). Figure 1 shows this forecast.

Figure 1 – Forecast of global oil and gas production growth trend.

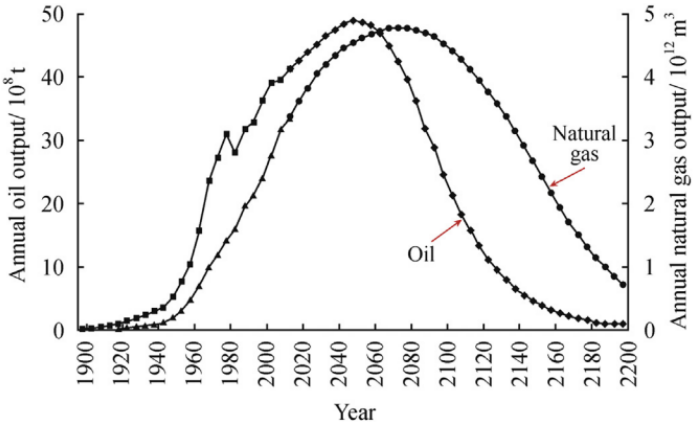

Source: (Zou et al., 2016).

Although Figure 1 shows that the decline in oil production should only occur around 2050, new technologies capable of exploring new mechanisms to serve as an alternative to fossil fuels could emerge at any time. The emergence of such a technology could anticipate this decline in the coming years resulting in the end of a multi-billion dollar industry. This potential fragility, together with the objective of prolonging the life of the economy based on the exploitation of oil and derivatives, has encouraged large investments as a way to improve processes and solve problems (Mancini & Paz, 2018; Sabet et al., 2018). This type of strategy promotes an increase in the competitiveness of petroleum derivatives (Mancini & Paz, 2018; Sabet et al., 2018), especially in sectors that are more sensitive to the emergence of new competing technologies, such as the fuel industry, which has recently started to compete with the popularization of electric cars (Cihat Onat et al., 2020). In addition, activities such as prospecting and transport also benefit, as in addition to investments encouraging increased production, they also improve process safety, mitigating the environmental impacts associated with the sector's activities (AlKazimi & Grantham, 2015; Cordes et al., 2016).

2.1.1 The Fuel Adulteration Problem

One of the main problems faced by the oil and gas sector is fuel adulteration. Unlike contamination, where one or more substances are inadvertently added to the fuel, adulteration is defined as the intentional addition of substances, usually with the aim of increasing the volume available for sale (Vempatapu & Kanaujia, 2017). This practice is possibly present in all countries where combustion systems are used, since studies that address this type of problem

in different countries are easily found in the literature(Gawande & Kaware, 2013; Kalligeros et al., 2003).

In addition to adulteration not being a problem limited to a single country or region (De Paulo et al., 2012), combating this problem is particularly complex due to the different methodologies employed by adulterators (Vempatapu & Kanaujia, 2017). Based on this scenario, numerous techniques can be found in the literature, usually applicable within the context of a specific type of analysis (Vempatapu & Kanaujia, 2017). In addition, most of these techniques are restricted to laboratories since they depend on complex procedures and human resources with prior training, such as chromatography (Majhi et al., 2011) and spectroscopy (Ferreiro-González et al., 2014). This large number of approaches, together with the high degree of specificity involved, reveals the level of difficulty involved in combating fuel adulteration. Figure 2 lists some of the main tests used to detect gasoline and diesel adulteration.

Figure 2 – Some test methods for monitoring gasoline and diesel adulteration.

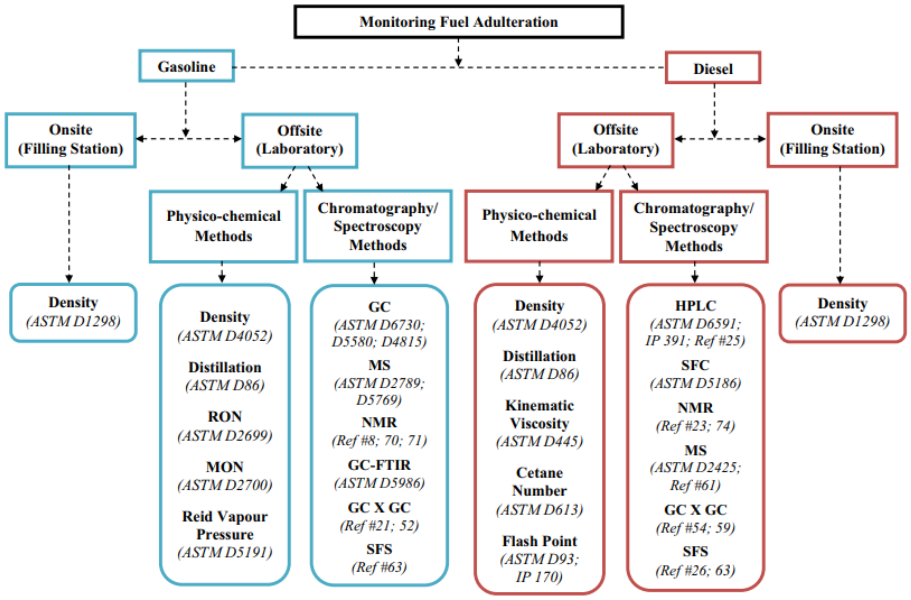

Source: (Vempatapu & Kanaujia, 2017).

As illustrated in Figure 2, analyses outside the laboratory environment are restricted to measuring sample density. Although this methodology is not capable of identifying the nature of a possible adulterant, it constitutes an important quality indicator and can even be performed by the customer, due to its simplicity.

Another important point regarding fuel adulteration is its multiple harmful effects (De Paulo et al., 2012). These effects go beyond the economic barrier, promoting a considerable

increase in the levels of polluting gas emissions, such as CO and NO_x (De Paulo et al., 2012; Vempatapu & Kanaujia, 2017). The social impacts of this practice are also extremely harmful since the unfair competition resulting from adulteration reduces tax collection and affects large and small businesses, in addition to potentially generating high costs for consumers (De Paulo et al., 2012). The latter is especially affected since the use of adulterated fuels contributes to reducing the useful life of the combustion system components and significantly reduces its efficiency (De Paulo et al., 2012).

In addition to resulting in different harmful effects on society and the environment, another feature of fuel adulteration is the variability of substances used as adulterants (Vempatapu & Kanaujia, 2017). In the case of diesel, for example, there are reports of adulteration through the addition of kerosene, vegetable oils or automotive lubricants (Brandão et al., 2012; Corgozinho et al., 2008; Cunha et al., 2016). The use of kerosene as an adulterant is especially attractive because, in addition to having a low cost, it is chemically similar to diesel, with similar sizes among its hydrocarbons (Vempatapu & Kanaujia, 2017).

Although gasoline can also be adulterated with the addition of kerosene or similar, ethanol has emerged as an important adulterant in some specific countries such as Brazil, Canada, Paraguay, Chile and Argentina (Bezerra et al., 2019). This happens because Brazilian legislation, for example, pre-establishes the addition of ethanol to gasoline, where around 27% of the total volume of the mixture must be composed of ethanol, in order to mitigate the environmental impacts resulting from emissions from combustion engines (Bezerra et al., 2019). This percentage of ethanol in gasoline favors adulteration through the addition of more ethanol to the fuel mixture since it is a cheaper biofuel.

In addition to petroleum-derived fuels, biofuels such as ethanol are also subject to adulteration (Vello et al., 2017). For this specific case, water is usually the most viable alternative as an adulterant due to its ease of obtaining, its good miscibility in mixtures with alcohol and the absence of color or characteristic smells that could contribute to the visual identification of a possible adulterated sample (Vello et al., 2017). Another aggravating factor for this specific adulteration is the damage resulting from the excessive presence of water molecules (Matějovský et al., 2017). In these cases, problems such as corrosion are accentuated since ethanol enhances the corrosive action of the mixture by increasing the water solubility and changing the electrochemical properties of the mixture (Matějovský et al., 2017).

2.1.2 Use of fertilizers in the production of biofuels

Although at first sight, the management of fertilizer use seems to be a problem far from the oil and gas industry, it is a particularly challenging scenario in the context of biofuel production (Otto et al., 2022). This connection stems from the fact that a significant part of the production of these fuels, such as the aforementioned ethanol, is produced from the cultivation of plants such as corn and sugarcane (Otto et al., 2022). Moreover, the distance between ethanol production and traditional fuels is progressively reduced as these alternative technologies are absorbed by the sector. A good example of this absorption is the addition of ethanol to gasoline, aiming at mitigating environmental damage related to the emission of pollutants, a strategy already mentioned (Bezerra et al., 2019).

Similar to other types of vegetable cultivation, fertilizers can be used as a way to supplement the supply of nutrients, ensuring the good development of the plant and, consequently, good production rates (Otto et al., 2022). Despite the benefits, the indiscriminate use of fertilizers can promote an effect contrary to that desired with the production of biofuels, resulting in severe environmental damage, including an increase in emissions (Otto et al., 2022; Ruan et al., 2016).

The supplementation of nutrients through fertilizers can occur under different methodologies since different crops have different needs. Still, dependence on nutrients such as nitrogen (N) and sulfur (S) is present in all crops, stimulating studies on topics such as the development of new fertilizers and the impact of adding these compounds to the local ecosystem (Otto et al., 2022; Ruan et al., 2016).

Specifically, in the case of nitrogen, it is a nutrient associated with most of the biological components that support the processes associated with plant development (Gowariker et al., 2009). This nutrient is present in amino acids, proteins, chlorophyll, nucleic acid, and hormones, among many other substances (Gowariker et al., 2009). Due to this importance, most of the efforts involved in the use of fertilizers aim to increase the availability of absorbable nitrogen in the soil (Gowariker et al., 2009). This occurs because, although the soil normally has a large concentration of this nutrient, plants obtain this component mostly in the form of nitrate ions (NO_3^-) (Gowariker et al., 2009). In addition, this great importance makes it the target of intense competition not only by plants but by microbes that also depend on this component (Gowariker et al., 2009).

Although sulfur is commonly secondary to the role of nitrogen, this element is also extremely important for plant development, since it is present in different biological processes

(Gowariker et al., 2009). It has a remarkable role in the synthesis of amino acids, in addition to playing an important role in the conformation of proteins (Gowariker et al., 2009). It is also worth highlighting its direct participation in the photosynthetic mechanism, allowing the plant to develop properly (Gowariker et al., 2009). Like nitrogen, this nutrient is not absorbed in its monatomic form, having the sulfate ion (SO_4^{2-}) as its main precursor. Another important link with nitrogen is the apparent correlation between sulfur availability in the soil and the level of nitrogen uptake (Bologna-Campbell et al., 2013; Gowariker et al., 2009). Although more recent studies claim that these are independent processes, previous studies show that nitrogen absorption becomes limited due to the unavailability of sulfur in the soil (Bologna-Campbell et al., 2013; Gowariker et al., 2009).

One of the great challenges faced by producers of biofuels such as ethanol is in the management of these fertilizers. Although the use of fertilizers below the recommended minimum volume may not have the desired effect resulting in economic losses, the excess of fertilizers may be associated with even more severe effects (Bologna-Campbell et al., 2013) From a productive point of view, taking sugarcane as an example, excess nitrogen in the soil can affect plant development and the availability of sugar in the plant pulp, affecting ethanol production (Bologna-Campbell et al., 2013). In the environmental context, excessive use of fertilizers can result in various types of environmental impacts such as contamination of groundwater (Ruan et al., 2016). In addition, excessive use of fertilizers also directly stimulates the production of oxide nitrous (N_2O), a gas with a global warming potential 300 times greater than carbon dioxide (Otto et al., 2022). Figure 3 shows the correlation between over application of fertilizers and the N_2O emission rate.

Figure 3 – Balanced median N_2O emission rates as a function of applied N.

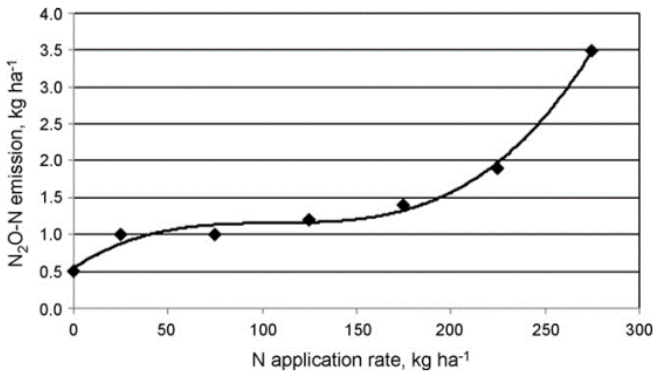

Source: (SNYDER et al., 2009).

The curve shown in Figure 3 was constructed by measuring emissions from different fertilized fields (Snyder et al., 2009). From this curve, it is possible to verify the existence of an inflection region, where the emission rate starts to grow rapidly with the application of fertilizer. The existence of this region emphasizes the importance of solutions capable of providing precise control over the use of these substances.

2.1.3 Challenges in Managing Pipelines and Mitigating Leak

Another important challenge faced by the oil and gas sector is the management of pipelines used to transport production. Transport by pipelines is one of the main methodologies used because it presents a high degree of efficiency since a large volume can be transported over long distances, at a relatively low cost when compared to other methodologies, such as transport by railways and highways (Korlapati et al., 2022; Senouci et al., 2014). In addition to being efficient, the use of pipelines is also associated with a high degree of reliability, resulting in a low failure rate when well managed (Badmos et al., 2009; Boaz et al., 2014). Still, despite being efficient and reliable, pipelines are susceptible to failure like any other system, but with the aggravating factor that, in case of serious accidents, these failures can result in major environmental disasters and economic losses (Senouci et al., 2014).

An important type of failure within the context of pipelines used for transportation is leaks (Boaz et al., 2014; Korlapati et al., 2022). This type of failure can be defined as a punctual and localized rupture of the body of a pipeline allowing the transported material to escape or the entry of some substance from the external environment (Wang & Duncan, 2014). Specifically for the oil and gas context, it makes sense to associate leaks with production leakage, considering that the process of transporting oil and its derivatives is carried out under great pressure, preventing any flow from outside to inside the pipeline.

The importance associated with the detection and location of these leaks is based on the ability of these small fractures to progressively evolve, which may result in ruptures in the most serious cases, resulting in the complete unfeasibility of the affected sector (Badmos et al., 2009; Wang & Duncan, 2014). In addition, the progressive loss of transported material also has several consequences for production efficiency, as it reduces the final volume of material produced and results in reduced pressure in the pipelines, making transportation difficult (De Sousa & Romero, 2017). From an environmental point of view, even small leaks can result in severe damage to the local ecosystem (Nambi et al., 2017; Zabbey & Olsson, 2017). While leaks in onshore operations can promote the formation of craters or the contamination of

groundwater (Bonnaud et al., 2018; Nambi et al., 2017), in offshore operations, they can mean the contamination of the entire food chain, resulting in the death of animals and, ultimately, in the contamination of people who come to consume some of these animals (Zabbey & Olsson, 2017).To mitigate the risks associated with this type of failure, different methods are employed to collect information in real-time, allowing the quick detection of any indication of leaks (Boaz et al., 2014; Korlapati et al., 2022). Table 1 exemplifies some of these methods.

Table 1 – Some methods used in leak detection and location.

Non Continuous	**Continuous**	
	External	**Internal**
Smart Pigging	Optical fiber sensor	Pressure point analysis
Inspection by helicopter, UAV, robots or similar	Acoustic sensor	Mass balance method
	Sensor hose	Statistical system
Trained dogs	Video monitoring	RTTM and E-RTTM System

Source: Adapted from (Boaz et al., 2014).

As shown in Table 1, it is possible to classify the methods used according to the continuity of their use (Boaz; Kaijage; Sinde, 2014). Non-continuous methods are, in general, techniques used without the need to monitor the operational parameters associated with the flow of production through the pipelines, and can also be used to better diagnose a possible failure previously located by other methods (Boaz; Kaijage; Sinde, 2014; Korlapati et al., 2022). Continuous methods, in turn, are methodologies developed to evaluate the functioning of the network while it is in operation. Some of these methods, such as the use of optical fiber sensors, allow this type of evaluation in real-time, optimizing the decision-making process (Korlapati et al., 2022).

Specifically for continuous methods, it is common to classify them as internal and external (Boaz; Kaijage; Sinde, 2014). Internal methods are usually associated with computational models applied to operational parameters obtained by sensing (Korlapati et al., 2022). These models seek to identify patterns that may be associated with events such as leaks (Korlapati et al., 2022). External methods, in turn, can be associated with direct detection through dedicated sensors or imaging systems, often without the need for a specific algorithm like those used by internal methods (Korlapati et al., 2022).

Leaks in pipelines can occur as a result of events of different natures, such as environmental disasters, mechanical failures and sabotage (Senouci et al., 2014). One of the

main causes of this type of incident is the chemical wear suffered by the walls of the pipelines through the progressive corrosion of the structure of the pipeline (Badmos; Ajimotokan; Emmanuel, 2009). This process, together with mechanical failures and incidents associated with third parties, is responsible for more than 80% of recorded failures (Senouci et al., 2014). Figure 4 shows the percentage distribution of the main causes associated with pipeline failures.

Figure 4 – Distribution in percentage of the main responsible for the occurrence of failures in the pipeline network.

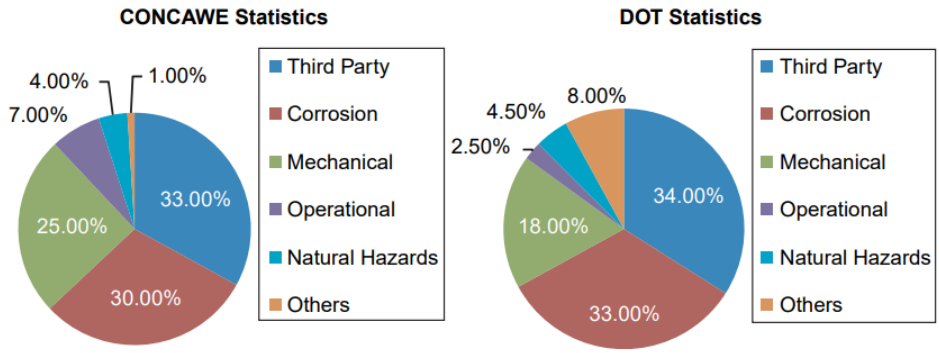

Source: (Senouci et al., 2014).

Although the problems responsible for the occurrence of leaks are well known, the plurality described in Figure 4 may suggest the impossibility of developing a single solution capable of covering all the problems pointed out. Instead, more specific strategies, such as cathodic protection in the case of corrosion, seem potentially more interesting (Senouci et al., 2014). For this second scenario, the most efficient generalist strategy possible is detection based on continuous monitoring of the pipelines. This type of methodology allows early intervention, mitigating economic losses and environmental damage (Boaz; Kaijage; Sinde, 2014).

2.2. OPTICAL FIBER SENSORS IN OIL AND GAS INDUSTRY

As already mentioned, optical fiber sensors are present in the oil and gas industry as one of the main solutions used for continuous sensing of pipelines (Korlapati et al., 2022). In addition to this scenario, this type of technology can also be found applied to several other types of sensing (Ashry et al., 2022; Edouard et al., 2022). In order to better assess the current context of optical fiber devices applied to the oil and gas industry, this section begins with a brief bibliometric analysis.

2.2.1 Bibliometric Analysis of Optical Fiber Sensors within the context of the Oil and Gas Industry

Bibliometric analysis is a methodology capable of providing important information from a large set of data obtained from scientific databases (Donthu et al., 2021). Through this methodology, it is possible to establish precise diagnoses regarding a given topic, identify possible trends and assess the impact of a specific contribution (Donthu et al., 2021). Given the versatility of this tool, it can operate on a large dataset, assuming high levels of complexity (Donthu et al., 2021). Despite this potential, a simple bibliometric analysis is described in this section to assess the main trends regarding fiber optic sensors within the context of oil and gas.

The first step in constructing the bibliometric analysis was the definition of the database and the researched terms. The selected database was SCOPUS (Elsevier) and for the choice of terms three research centers were defined: sensors, optical fibers, and the oil and gas industry. The definition of these three nuclei allowed for greater precision in the search for works, since only works inserted in these three themes were considered simultaneously. The first core was built from the search for terms such as "sensor", "sensing", "transducers" and similar. The second core addressed variations such as "optical fiber" and "fiber optics". Finally, the last nucleus used terms such as "oil and gas industry", "petroleum industry" or "oil industry". After this filtering, about 327 scientific papers were obtained.

Using the VOSviewer software, the correlations between the keywords of each of the 327 papers were evaluated, seeking to assess the magnitude of the correlations between each of the keywords. To increase the accuracy of the process, a new filtering step categorized the keywords, avoiding the repetition of equivalent terms and removing those that appeared in isolation. From this process, the diagram shown in Figure 5 was constructed.

From Figure 5, it is already possible to clearly observe the predominance of sensors based on the Fiber Bragg Grating (FBG) structure. In this Graph, the lines that connect the circles represent the correlation between the terms, as well as the size of these elements are associated with the frequency in which the terms were found during the bibliometric analysis. The FBG sensors are devices manufactured by exposing the core of the optical fiber to the signal emitted by a high-power laser (Edouard et al., 2022). This exposure locally increases the refractive index, allowing the modulation of an optical signal from the effective refractive index of that region (Edouard et al., 2022). As different parameters can be associated with these variations, these sensors can be used in different contexts, such as in gas flow detection (Cheng et al., 2011). This versatility allows its use in the monitoring of pipelines and wells (Cabral et

al., 2020; Zhang; Zhong; Li, [s.d.]), as a leak detector or in the detection of magnitudes such as temperature, pressure and flow velocity (Cabral et al., 2020; Lotfi; Noori, 2021; Zhou; Yu; Peng, 2019). Figure 6 shows highlighted keywords linked to FBG sensors.

Figure 5 – Bibliometric map built from the keywords of the works found.

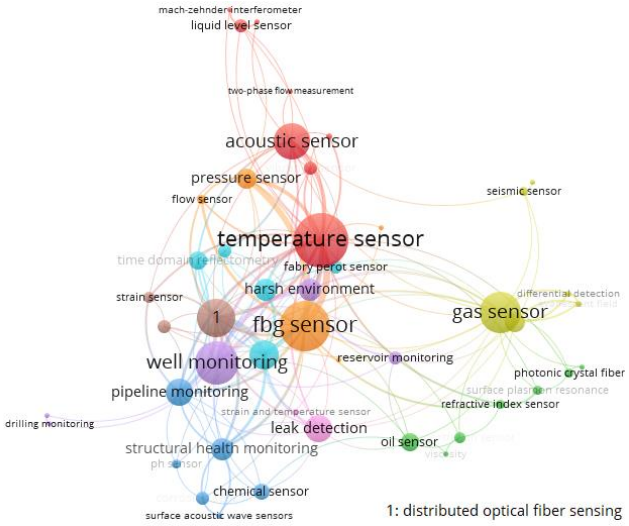

Source: Produced by the Author.

Figure 6 – Bibliometric map focusing on keywords related to the term "FBG sensor".

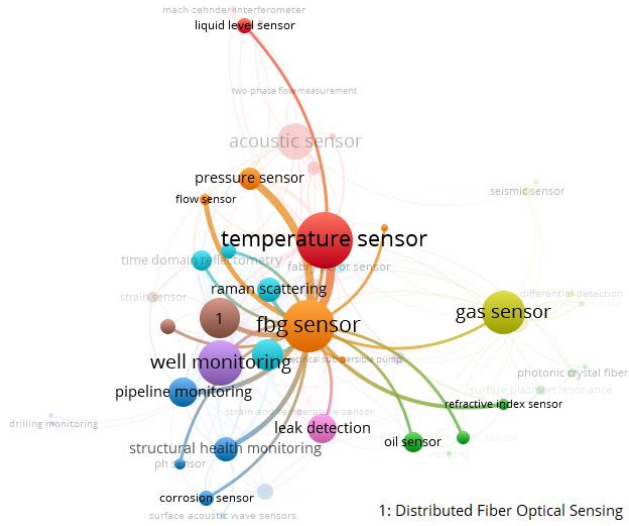

Source: Produced by the Author.

From Figure 6, it is possible to observe more clearly the correlation between the terms "fbg sensor" and "distributed optical fiber sensing". This correlation is important, as it demonstrates the feasibility of integrating FBG sensors into distributed measurement systems

(Zhong et al., 2021). In addition to FBG sensors, other methodologies can be employed to produce distributed sensors, such as the use of non-linear effects inherent to optical fiber, for example, Raman scattering (Peixoto E Silva et al., 2021). In the latter case, it is common to use techniques capable of providing the spatial location of sensed events, such as optical time-domain reflectometry (OTDR) (Peixoto E Silva et al., 2021). This technique will be presented and discussed in more detail in later chapters. Figure 7 shows the representation of the bibliometric map focusing on the term "distributed optical fiber sensing".

Figure 7 – Bibliometric map focusing on keywords related to the term "distributed optical fiber sensing".

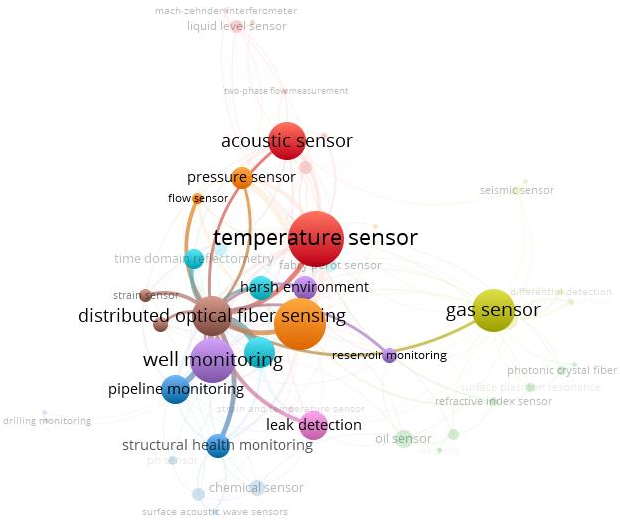

Source: Produced by the Author.

Similar to the map referring to the term "fbg sensor", Figure 7 shows that distributed sensing has strong appeal in the context of the oil and gas industry. This type of prominence is expected, since this sector has numerous assets with high added value organized in kilometers-long networks, making the use of point sensors unfeasible (ASHRY et al., 2022).

Two basic types of distributed sensing stood out during the bibliometric analysis: distributed temperature sensing (DTS) and distributed acoustic sensing (DAS). These methods have enormous prominence because, in addition to the favorable context, they are linked to different applications (Inaudi; Belli; Walder, 2008; Zhong et al., 2021). The DTS, for example, can be used to obtain the spatial profile of the temperature of a network of pipelines, while it can also be used to detect leaks since the escape of the material promotes local temperature variations (Inaudi; Belli; Walder, 2008).

Although some papers were found involving measurements of refractive index, surface plasmon resonance and other subjects commonly correlated with D-shaped optical fiber sensors, no papers were found about these devices. This lack of results does not necessarily imply the originality of the theme addressed by this dissertation, since the analysis carried out, in addition to being limited, had as its main purpose to evaluate the general context of fiber optic sensors applied to the oil and gas industry. Even so, it is possible to diagnose an incipient scenario that makes it possible to point out the consolidation of D-shaped optical fibers as technological solutions for the oil and gas industry as one of the main contributions of this work.

2.3. THE FUNCTIONING OF OPTICAL FIBER AND THE EVANESCENT WAVE

Before presenting more details about the theory behind the proposed sensor, it is important to understand some basic principles that underpin the functioning of the optical fiber as a device. Optical fiber is a device made of transparent material whose operating principle is based on the physical phenomenon known as total internal reflection (TIR) (Agrawal, 2019). This phenomenon occurs when an electromagnetic wave (EW) cannot cross the interface that separates two media, being reflected back to its source medium (Agrawal, 2019). It is usually described mathematically as a special case of the Second Law of Refraction (Agrawal, 2019), also known as the Snell-Descartes Law, given by

$$n_1 \cdot \sin\theta_1 = n_2 \cdot \sin\theta_2 \tag{1}$$

where n is the index of refraction, θ is the angle between the incident EW and the normal line to the interface that separates the media, referenced by subindex 1 and 2. It is assumed that subscript 1 is associated with incident EW, while subscript 2 is associated with refracted EW.

To observe the occurrence of TIR from the Snell-Descartes Law, the EW must propagate from the more refractive medium, with a higher refractive index, to the less refractive medium, with a lower refractive index (Agrawal, 2019). In this case, the Snell-Descartes Law can be rewritten as

$$\sin\theta_2 = \frac{n_1}{n_2} \cdot \sin\theta_1 \tag{2}$$

from where it is possible to observe that

$$\frac{n_1}{n_2} > 1 \rightarrow \sin\theta_2 > \sin\theta_1 \rightarrow \theta_2 > \theta_1 . \quad (3)$$

This consideration shows that when an EW undergoes refraction from a more refractive medium to a less refractive medium, the angle that the EW makes with the normal line to the surface increases, resulting in an angular departure from this line (Agrawal, 2019). This behavior suggests that there is an angle of incidence such that the EW cannot cross the interface, propagating parallel to it. This incidence angle, which results in a refraction angle equal to 90 degrees, is called the limit angle, since any angle greater than this angle produces the phenomenon of total internal reflection (Agrawal, 2019). In this case, the incident wave is reflected back to its source medium. Figure 8 illustrates different types of incidences.

Figure 8 – Different types of incidences of an electromagnetic wave traveling from a more refractive medium to a less refractive one.

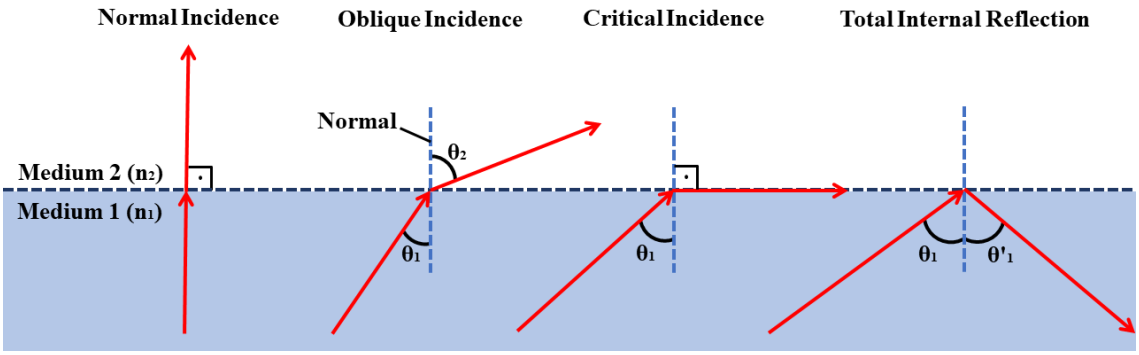

Source: Produced by the Author.

To ensure that the total internal reflections occur throughout the optical fiber, regardless of the refractive index of the external medium, the optical fiber is usually composed of two materials (Agrawal, 2019). The first of them called the core, has a high refractive index and a low attenuation coefficient, as it is through it that the optical signal propagates (Agrawal, 2019). The second material, called cladding, has a lower refractive index than the core and is arranged in such a way as to encapsulate and isolate it from the external environment (Agrawal, 2019). This isolation guarantees the essential condition necessary for TIR occurrence, regardless of the external environment.

The presence of the cladding also contributes to the increase in mechanical strength and, in multimode fibers, directly impacts the numerical aperture, a property that defines the range of angles that the optical fiber can guide (Agrawal, 2019). For glass optical fibers, the presence of the cladding is also capable of correcting imperfections characteristic of the fabrication

process, mitigating the attenuating action resulting from the presence of cracks and pores (Agrawal, 2019; Fontana, 2021). Figure 9 shows a cross section of the two different optical fiber technologies used in this work: plastic optical fiber (POF) and single-mode optical fiber (SMF) at scale.

Figure 9 – Comparison between cross section dimensions of a plastic optical fiber and single-mode optical fiber.

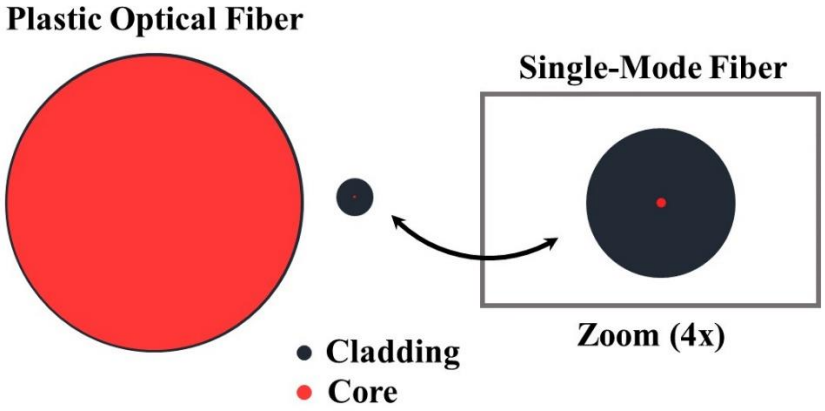

Source: Produced by the Author.

An important aspect of fiber-guided optical signal propagation is that, counterintuitively, the optical power in the vicinity of the core-cladding interface is not zero as shown in Figure 10. This is because, although the Snell-Descartes Law does not suggest other consequences during the occurrence of reflections, the optical signal as an electromagnetic wave is also subject to other mathematical relationships when it affects the interface: the Maxwell Equations (Fontana, 2021). These equations are given by

$$\vec{\nabla} \times \vec{E} = -\frac{\partial \vec{B}}{\partial t} \tag{4}$$

$$\vec{\nabla} \bullet \vec{D} = \rho \tag{5}$$

$$\vec{\nabla} \bullet \vec{B} = 0 \tag{6}$$

$$\vec{\nabla} \times \vec{H} = \vec{J} + \frac{\partial \vec{D}}{\partial t} \tag{7}$$

where alternatively they are known as Faraday's Law, Gauss's Law, Gauss's Law for magnetism and Ampere's Law, respectively (Fontana, 2021). The meaning of the symbol presented by the equations is described in Table 2.

Table 2 – Physical quantities present in Maxwell's 4.

Symbol	Description
$\vec{E}$	Electric field vector
$\vec{D}$	Electric flux density vector
$\vec{B}$	Magnetic flux density vector
$\vec{H}$	Magnetic field vector
$\vec{J}$	Current density vector
ρ	Charge density

Source: Adapted from (FONTANA, 2021).

As the material media where, electromagnetic waves propagate have intrinsic electromagnetic properties, in addition to Maxwell's Equations, two other expressions are of great importance for the construction of an understanding of how the signal traveling in the optical fiber interacts with the waveguide while electromagnetic wave (Agrawal, 2019; Fontana, 2021). These are called constitutive relations and are given by

$$\vec{D} = \varepsilon_0 \vec{E} + \vec{P} \tag{8}$$

$$\vec{B} = \mu_0 (\vec{H} + \vec{M}) \tag{9}$$

where ε_0 and μ_0 are, respectively, the permittivity and the permeability of free space. In addition, $\vec{P}$ represents the polarization vector while $\vec{M}$ represents the magnetization vector.

Figure 10 – Optical signal propagating confined within an optical fiber with emphasis on power distribution.

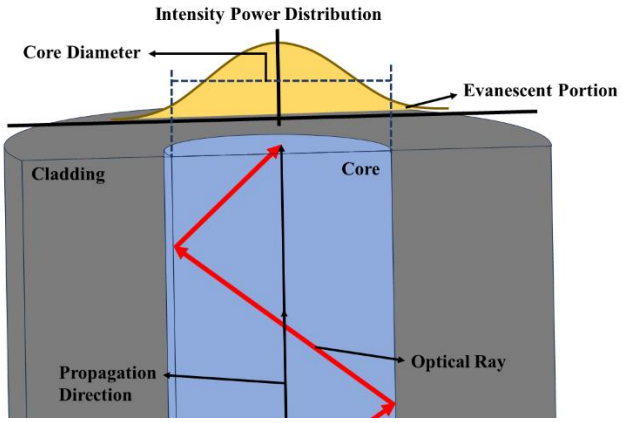

Source: Produced by the Author.

Finally, using these six expressions it is possible to arrive at two new expressions known as boundary conditions. These new expressions are able to explain the existence of this residual optical power, concentrated right after the core-cladding interface. They are given by

$$\hat{n}\bullet(\vec{B}_2 - \vec{B}_1) = 0 \tag{10}$$

$$\hat{n}\bullet(\vec{D}_2 - \vec{D}_1) = \rho_s \tag{11}$$

with ρ_s representing the surface charge density. As in the case of optical fiber the surface in question separates two dielectrics, we have

$$\hat{n}\bullet(\vec{D}_2 - \vec{D}_1) = 0 \tag{12}$$

This last expression indicates that both the electrical component and the magnetic component of the signal that propagates in an optical fiber must remain continuous, resulting in the appearance of this residual optical power. As this power appears in the form of an electromagnetic field that, in addition to rapidly decaying with distance, propagates together with the optical signal, this field is called an evanescent wave (Alves, 2020).

Despite the optical power associated with the evanescent wave being significantly lower and decaying with distance, this is a phenomenon widely explored for the construction of optical devices (Alves, 2020). These difficulties can be circumvented through different methodologies, including the one that will be proposed in this work in future chapters, since the proposed device is fundamentally based on the interaction between the evanescent wave and the external environment.

2.4. D-SHAPED OPTICAL FIBERS

A possible strategy to enable the interaction between the evanescent wave and the parameters of the external environment is to partially or completely remove the optical fiber cladding. This removal can be performed using different techniques and methodologies, resulting in optical fibers with different geometries (Alves, 2020). Within this class of devices, D-shaped optical fibers (OF-Ds) stand out because, among other things, they have a flat surface that is especially favorable for the deposition of different substances. The availability of this substrate inherent to the device allows the creation of complex sensors capable of detecting the

most diverse types of compounds with a high degree of specificity (Alves, 2020). The OF-Ds receive this name due to the similarity of the geometry of its transverse section to a letter D, as illustrated in Figure 11.

Figure 11 – Cross-section of a D-shaped single-mode optical fiber (SMF-D) and a D-shaped plastic optical fiber (POF-D). Dimensions out of scale.

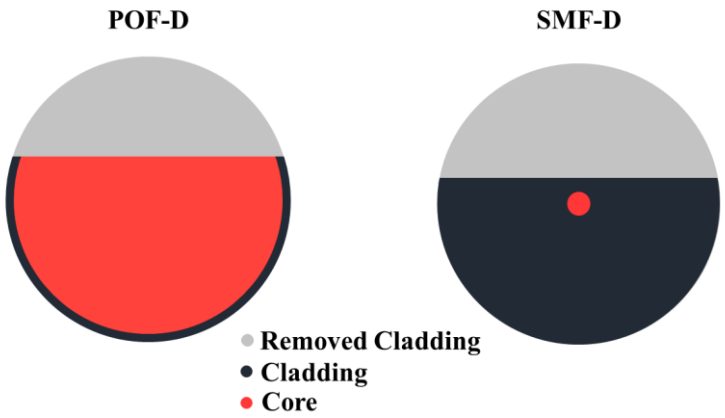

Small variations can be found, normally associated with geometric parameters for the device, such as residual cladding thickness or the D-shaped length. A good example of these variations is in the specific case of POFs, where not only the cladding is fully removed, but also part of the core. As will be discussed below, these geometric parameters are fundamental to characterization of these devices, as they directly impact the final response of sensors (Barros et al., 2022a).

2.4.1 D-shaped Optical Fiber Structure

In addition to the use of OF-Ds as detectors through the deposition of substances, several other technologies can be used in conjunction with this structure, making it a versatile solution for a wide range of problems (Alves, 2020). OF-Ds can be used coupled with planar waveguides, for example, allowing the device to be sensitized through particular properties of the propagating medium of the planar waveguide (Alves, 2020). Bragg grating structures can also be inserted into OF-Ds for the detection of, among other things, mechanical deformations or the construction of interferometers (Alves, 2020).

Different optical fiber technologies can be used beyond to traditional D-shaped single-mode optical fibers (SMF-D), further expanding the possible applications (Barros et al., 2021). D-shaped plastic optical fibers (POF-Ds) are interesting alternatives due to their substantially

greater mechanical resistance and their high refractive index, and can be used in environments where traditional systems tend to have high optical loss, as in media with high value of refractive index (Barros et al., 2021, 2023a). Although in smaller numbers, experimental works are also found in the literature involving D-shaped photonic crystal fibers (PCF-Ds) (Alves, 2020). This structure, when applied to fluid media, allows direct interaction between these fluids and the optical signal, through the entry of fluids in the channels of the optical fiber (Alves, 2020).

Finally, it is worth mentioning that although OF-Ds can compose complex devices, their use without any additional structure is also feasible and widely found in the literature (Barros et al., 2022b). Often referred to as an exposed D-shaped, this configuration is used for applications where a high degree of specificity is not required, such as leak detection or level control in reservoirs (Barros et al., 2023b).

2.4.2 The Roughness Effect

Another important operational parameter in addition to the geometric parameters is the level of roughness on the flat face of the D-shaped optical fiber. The minimization of this parameter can be essential to ensure the operation of a device based on the deposition of some material on this surface. In addition, a regular surface also contributes to the non-adherence of materials on the surface, a common problem in refractive index measurements and which, in the last case, can completely passivate the sensor element, making the continuity of measurements unfeasible.

Roughness can also be desirable despite the previously described scenario, as it is capable of changing the sensor response in certain situations. Specifically in the case of optical fibers with an exposed D-shaped, this parameter allows the detection of refractive index variations that generally would not be detected in a roughness-free system. This behavior is commonly associated with promoting optical scattering over the flat surface, allowing the coupling of optical signals external to the optical fiber to the propagating sign in its core. This effect is illustrated in Figure 12.

Figure 12 – Representation of a longitudinal section of D-shaped optical fibers. (a) without roughness. (b) with roughness.

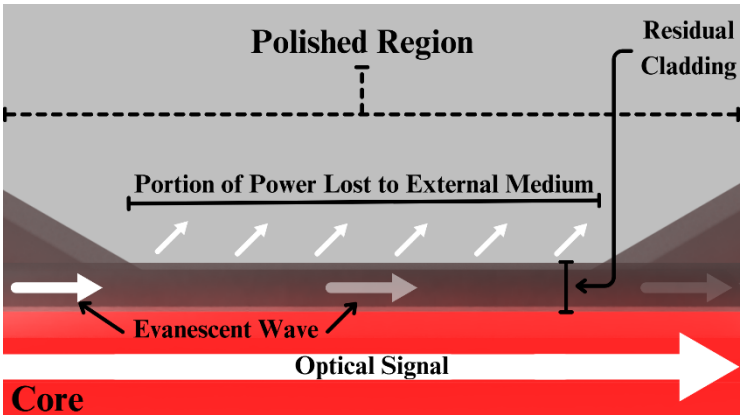

(a)

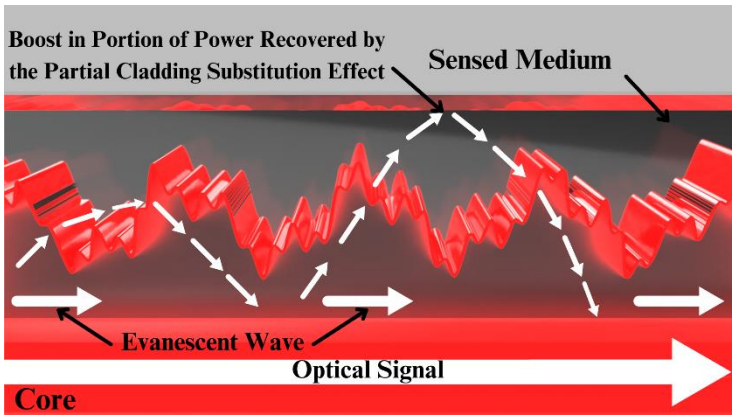

(b)

As shown in Figure 12, the presence of roughness on the flat surface of the OF-Ds provides a significant increase in the amount of radiation that interact with the external medium and returns to the core of the optical fiber (Alves, 2020). Upon arriving at the core of the optical fiber, this radiation is coupled to the optical signal, since it becomes subject to the condition of propagation through multiple TIRs. This coupling can be visualized in the form of optical gain and varies according to the refractive index of the external environment, allowing its measurement (Barros et al., 2021, 2022b).

3 SIMULATION, FABRICATION AND CHARACTERIZATION OF D-SHAPED OPTICAL FIBER SENSORS

This chapter provides details on optical fiber preparation, sensor fabrication, and the approach used during calibration and measurements. Section 3.1 details the sensor fabrication process, highlighting the instrumentation used in this process. In Section 3.2, a computational model created to represent the device's response is presented, in order to establish a reliable model capable of guiding the use of the manufactured sensors. Finally, Section 3.3 presents the characterization process, responsible for evaluating the response of the sensors produced and determining whether or not they should undergo new adjustments.

3.1. FABRICATION PROCESS OF D-SHAPED OPTICAL FIBERS

Different methodologies can be used to fabricate the D-shaped optical fibers, such as laser ablation or chemical-controlled etching (Alves, 2020). Each of these approaches has advantages and disadvantages, but the high degree of precision in process control tends to be a common point in all of them, mainly due to the physical dimensions of the optical fibers used. An interesting option in the face of this challenging scenario is mechanical polishing, as it does not require the use of potentially dangerous chemical reagents, for example. Due to these benefits and the simplicity of its implementation, this is the method adopted in this work. In the next section are presented details of the polishing system implemented.

3.1.1 Polishing System: Mechanical Components

The main component used in the proposed fabrication process is the ZFS25B nanometer stepper motor from Thorlabs Inc. It is responsible for allowing the operation with the optical fiber with the degree of precision of the order of micrometers necessary for the process. In addition to it, an AC motor, abrasive disk, a photodetector circuit, a control system and a light source that can be a laser or an LED depending on the type of optical fiber used are also used. This ability to work with different types of optical fibers, only needing to change the light source, also represents a strong point of mechanical polishing, considering that other methods such as chemical etching require a deeper reformulation to operate alternately with plastic optical fibers and single-mode optical fibers. The Figure 13 illustrates all the components used during the D-shaped optical fiber fabrication.

Figure 13 – Representation in the block diagram of the instrumentation used in D-shaped optical fibers fabrication.

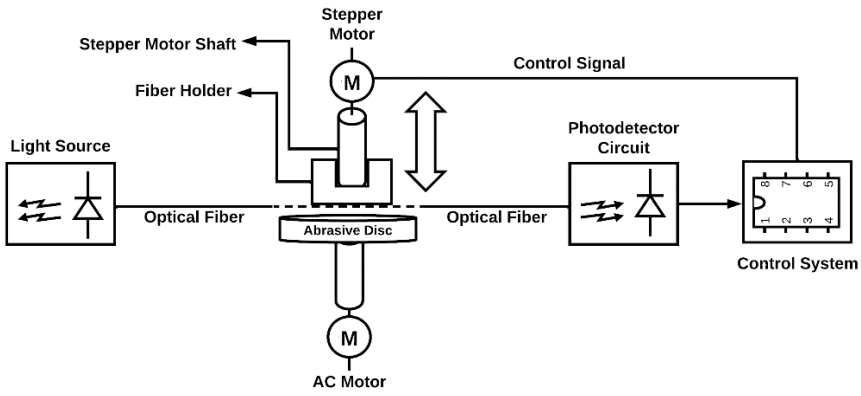

Source: Produced by the author.

As indicated in Figure 13, the basic principle of the methodology used is to use the stepper motor to bring the optical fiber closer to or farther from an abrasive disk coupled to the shaft of an AC motor. This disk is kept rotating at a constant speed and can be changed at any time, allowing control over the level of abrasion used and, consequently, the level of roughness of the polished surface. This control allows for optimizing the speed of the manufacturing process since more abrasive disks can be used initially and are sequentially replaced by less abrasive disks as the polishing progresses. This abrasive property is related to the presence of silicon carbide incrustations, a common abrasive in commercial sandpaper. Controlling the level of roughness of the polished surface also allows optimizing the response of the manufactured sensor, since this parameter results in an optical power gain in one of the sensor's operating ranges, as previously discussed.

An important detail that can also be seen in Figure 13 is that the optical fiber is coupled to the stepper motor shaft, but not directly, so a support is used to interface this attachment. The use of this support aims not only to improve the ability to fix the optical fiber on this shaft but also to increase the mechanical strength of the polished region and facilitate handling throughout the manufacturing process. This support consists of an acrylic substrate where the optical fiber is fixed using epoxy resin, a thermosetting polymer that hardens in the presence of a catalyst, acquiring mechanical, thermal and chemical resistance. Figure 14 shows optical fibers fixed on this type of substrate.

Figure 14 – Polished optical fibers fixed to the substrate.

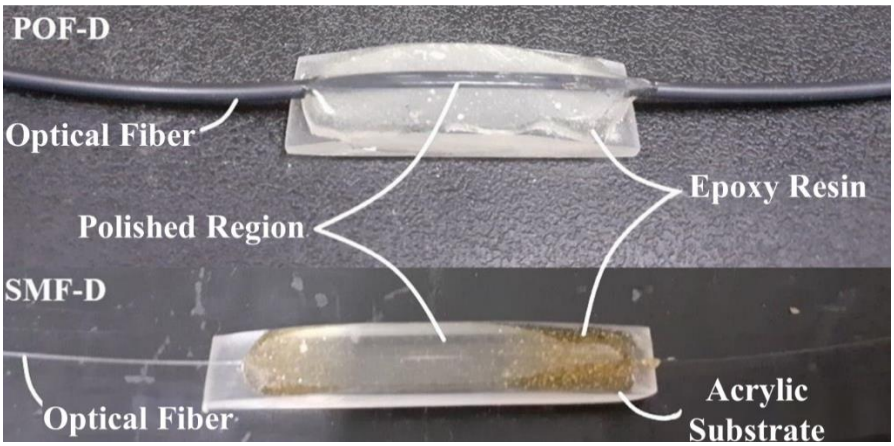

Source: Produced by the author.

These substrates, in addition to contributing to increased resistance and improved handling of the sensor element, are also used to define the geometry of the polished region. This is because the length of the D-shaped region is determined by the length of the flat region of the substrate, typically around 13 millimeters. Due to this correlation, substrate fabrication also becomes of great importance for sensor fabrication, since, as will be discussed below, the length of the polished region is a central parameter in sensor sensitivity.

3.1.2 Polishing System: Optical Power Meter

The management of the stepper motor movement is carried out entirely by an Optical Power Meter (OPM) developed specifically for the fabrication process. This device is composed of the light source, the photodetector circuit and the processing unit represented as a control system in Figure 13. The creation of this device was thought of bearing in mind the relationship between the depth reached by the polishing and the gradual optical signal that propagates to the external medium. This correlation is seen by the system as a progressive insertion of optical losses in the polished region, justifying the use of the light source and the photodetector circuit. The processing unit, in turn, consists of a single-board Arduino microcontroller which, through a routine implemented in software, determines whether the stepper motor should bring the polished region closer to or farther from the abrasive disk.

Two different light sources were used, the first being a laser that emits a continuous wave (CW) with a wavelength equal to 1310 nanometers. This source was used with single-mode silica optical fibers (SMF) and, as it has a wavelength in the center of the frequency range

known as the O-band, it is compatible with several optical devices, even the oldest ones. This flexibility allows exploring the use of the OPM and SMF-D in conjunction with other devices. This choice, although important for the analysis of the results, does not imply any type of limitation of the produced sensor, since the D-shaped optical fibers do not present any additional limitation in their transmission band.

The second light source was a HFBR-15X7Z transmitter manufactured by Avago Technologies, which consists of an LED encapsulated in a specific housing for connection with HFBR-4501Z connectors (Avago, 2012). The choice of this light source is aimed at its use in conjunction with plastic optical fibers (POF), allowing easy coupling and reducing the level of optical loss. Furthermore, the optical signal emitted with about 650 nanometers in wavelength also coincides with a region of low optical attenuation at plastic optical fibers, as shown in Figure 15.

Figure 15 – Attenuation behavior as a function of the transmitted optical signal wavelength for plastic optical fibers.

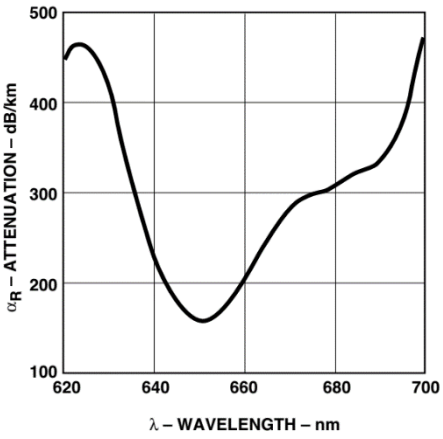

Source: (Avago, 2012).

As two different light sources were used, two photodetectors were also used, one 1310 nanometer InGaAs photodetector for the configuration used with the SMF-Ds and the HFBR-25X6Z receiver for the configuration used with the POF-Ds. This second photodetector consists of a 650 nanometer PIN photodiode with an integrated transimpedance preamplifier, also manufactured by Avago Technologies. The characterization process of these two pairs of light source-photodetector occurred in a similar way, using the commercial optical multimeter AQ2150A (Ando Electric Company). Initially, the operating current of the light sources was varied and the optical power measured by the multimeter was recorded, then the process was repeated, but this time recording the electrical voltage on the photodetector terminals. At the

end of these measurements, it was possible to establish an indirect relationship between the voltage response of the detectors and their correspondence in terms of optical power.

3.2. COMPUTATIONAL MODELING: D-SHAPED OPTICAL FIBER GENERAL MODEL

A computational model of D-shaped optical fibers was also developed in parallel to the sensors fabrication. This modeling was performed using the COMSOL Multiphysics software (version 5.6), which applies the finite element method to perform analysis and complex simulations of physical systems. This approach made it possible to consolidate the results obtained, in addition to enabling the construction of a consistent model that could be used in future studies. In addition, using a simulation of this size also offers the opportunity to explore in more detail the operation of D-shaped optical fibers, analyzing the effect of varying parameters or any differences between the experimental and computational models.

Using the COMSOL mode called “Electromagnetic Waves, Frequency Domain (ewfd)” included in the interface “Wave Optics”, two different models were built taking into account the need to consolidate the results obtained for each of the fibers used. Figure 16 illustrates the representation of the domains modeled for the construction of each of the simulations. These three represented domains are the core, the cladding and the external environment, all represented by circles. Finally, it is also worth mentioning that, for the model implemented in this work, the optical wave module was used, with the electromagnetic wave submodule in the frequency domain.

Figure 16 – Representations used in the COMSOL Multiphysics Software to model a (a) SMF-D and (b) POF-D, in both case with emphasis on them domains.

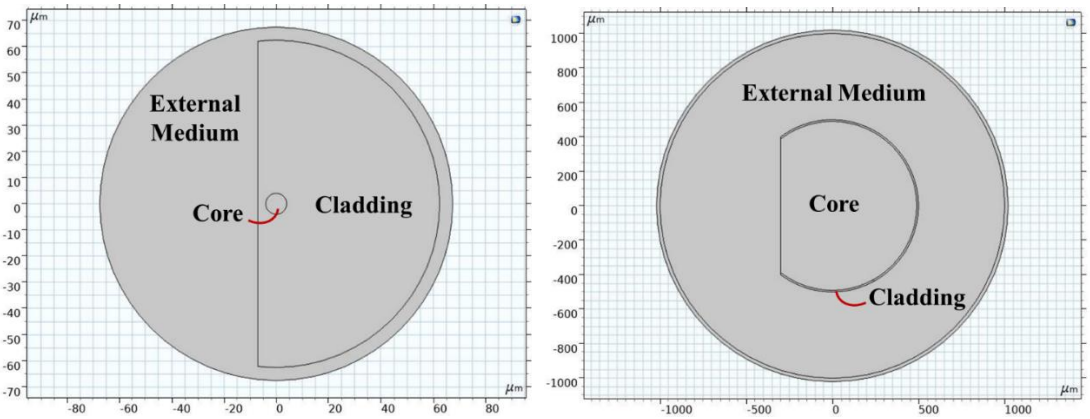

Source: Produced by the author.

The study to obtain the propagation modes in the SMF-D and POF-D structures was performed through modal analysis, which provides the effective refractive index associated with each propagation mode. The effective index of refraction is a functional of the form $n_{eff} = n_{eff}(\lambda, n_{core}, n_{clad}, n_{ext}, d)$, so it depends on the optical properties and geometry of the D-shaped fiber. Therefore, changes in the refractive index of the external medium can cause changes in the effective refractive index. Finally, the relative transmitted optical power is obtained in the simulation from the Transmittance (T), given by

$$T = \exp\left[-2\,\mathrm{Im}\left(n_{eff}\right)k_0 L\right] \tag{13}$$

where $\mathrm{Im}(n_{eff})$ is the imaginary part of the effective refractive index, k_0 is the wave number in a vacuum and L is the length of the D-shape. Finally, the parameters used in the construction of the two models are listed in Table 3.

Table 3 – Parameters used in the construction of computational models.

Parameters	**SMF-D**	**POF-D**
Core Refractive Index (n_{core})	1.4443 RIU	1.492 RIU
Cladding Refractive Index (n_{clad})	1.4378 RIU	1.417 RIU
Wavelength (λ)	1310 nm	650 nm
Core Diameter (d_{core})	8 μm	980 μm
Cladding Diameter (d_{clad})	125 μm	1000 μm

Source: Produced by the author.

From the configuration of the parameters described in Table 3, it is necessary to configure the parameters used in the discretization process implemented by the software: basically, the geometry to be used and the size of each of these elements. This discretization allows the software to transform large and complex areas into sub-areas of reduced size, facilitating the calculation of differential equations associated with simulated physics. For reasons of performance and conformation, given the circular geometry of the model, triangular elements were chosen for the discretization. The size of each finite element was adjusted according to its location in order to optimize the accuracy of the simulation, ranging from $\lambda/6$ to $\lambda/16$. Figure 17 (a) shows this discretization applied to the SMF-D model, while Figure 17 (b) shows the same for POF-D.

Figure 17 – Discretization through Finite Element Methods application by the software. (a) Discretization of SMF-D model. (b) Discretization of POF-D model.

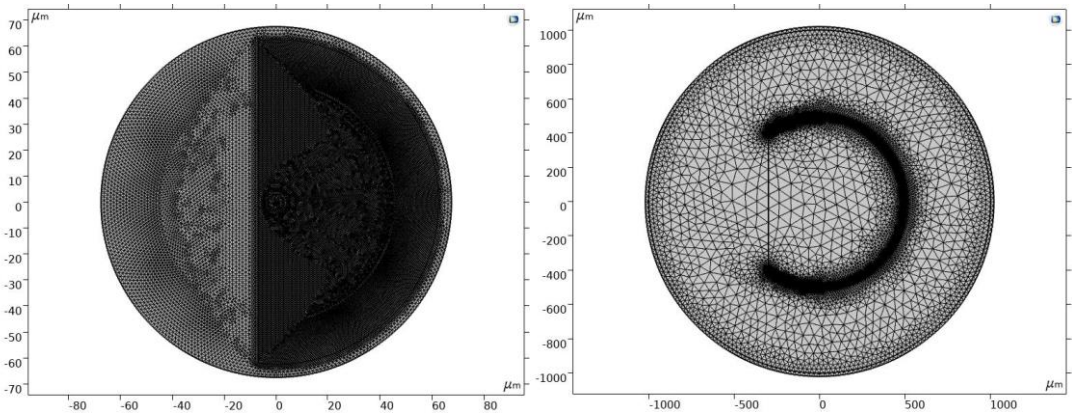

Source: Produced by the author.

According to Figure 17, it is possible to visualize that a greater number of elements were purposely positioned in the core-cladding interface. This practice occurs in view of the central role of the evanescent wave in the functioning of the device. In addition, the use of larger amounts of elements only in the core-cladding interface also allowed a drastic reduction in the consumption of computational resources, while not showing significant divergences from the model with uniform distribution of these elements across all domains.

The reduction in the use of computational resources can be seen as a one-off gain when modeling a single scenario. However, considering the expressive number of measurements carried out, with the use of different configurations for the parameters of the domain representing the external environment, the gains obtained with this economy of resources had their impacts amplified.

3.3. COMPUTATIONAL MODELING: ABSORPTIOMETER BASED ON SMF-D

Stimulated by the results obtained from SMF-D computational modelling, a study was also carried out to verify the possibility of using the sensor based on D-shaped fibers as an absorptiometer. The scenario investigated was the detection of ionic species linked to the use of fertilizers, to optimize their application. A device like this has the potential to reduce the costs and impacts of using fertilizers, as well as being strategic for the oil and gas industry in the production of biofuels such as ethanol from sugar cane.

Before modeling and getting the device response, a few distinct steps needed to be established for building a solid model. Initially, it was necessary to define the ionic species

evaluated, as well as their respective absorption coefficient (κ). The chosen species were the nitrate and sulfate ions coming from the ionic dissolution of ammonium nitrate (NH_4NO_3) and ammonium sulfate ($(NH_4)_2SO_4$), respectively. Figure 18 shows the relationship between the absorption coefficient of the chosen species for different wavelengths.

Figure 18 – κ values of aqueous solution of ammonium nitrate and ammonium sulfate, at different wavelengths and concentrations.

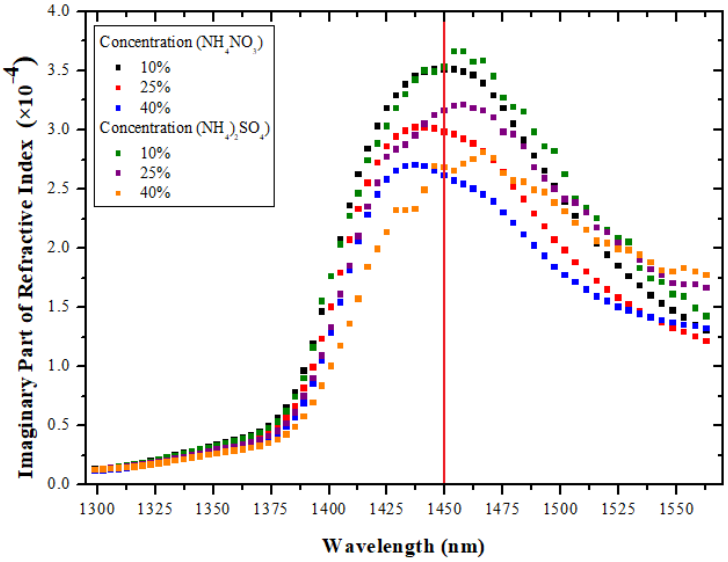

Source: (Barros et al., 2022a).

The choice of ionic species was based on the fundamental role of ammonia in the composition of nitrogen fertilizers, as well as on the physiological role of nitrate and sulfate ions for plants. As this is an exploratory conceptual study, the value chosen for the wavelength of the optical signal was 1450 nm, given its proximity to the peak of the κ values. The red line in Figure 18 indicates the location of the points at this wavelength. In addition, the choice of another wavelength in relation to the other studies presented in this work resulted in the need to change the refractive indices related to the optical fiber. For the SMF-D cladding the value used was 1.4434 RIU, and for the SMF-D core region the value was 1.4515 RIU. These values were obtained from the Sellmeier Equation (Brückner, 2011).

As this is an exploratory study, the influence of two of the most important geometrical parameters for the SMF-D was also addressed: the thickness of the residual cladding and the length of the D-shaped region. Thus, each of these parameters was changed progressively, in order to evaluate the influence of each of them on the final response of the device and to serve as bases for future work that can explore the fabrication of a device like this.

3.4. CHARACTERIZATION PROCESS

With the sensors fabricated and in possession of the computational results, the characterization of this sensor is carried out. This characterization is performed in two different steps: the determination of the OF-D geometrical parameters and the evaluation of the OF-D response. In the first step, the length of the polished region and the depth reached due to the polishing are determined using optical microscopy and digital image processing. Figure 19 shows an image from a POF-D obtained through microscopy.

Figure 19 – Image from POF D-shaped region after polishing obtained through optical microscopy.

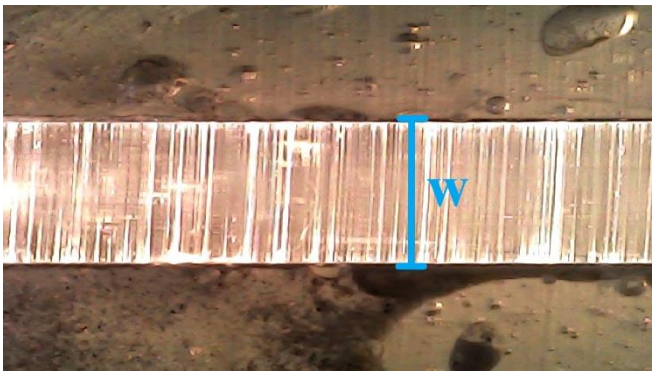

Source: Produced by the author.

The determination of the depth reached by polishing is possible using a simple math model that depends, besides the original geometric measurements, on the polished region width represented in Figure 19 by the blue line and the letter w. This math model is based on a Pythagorean relationship that can be best viewed from the cross-section of the polished region as shown in Figure 20.

Figure 20 – Geometric modeling used to calculate the depth reached through the polishing (d).

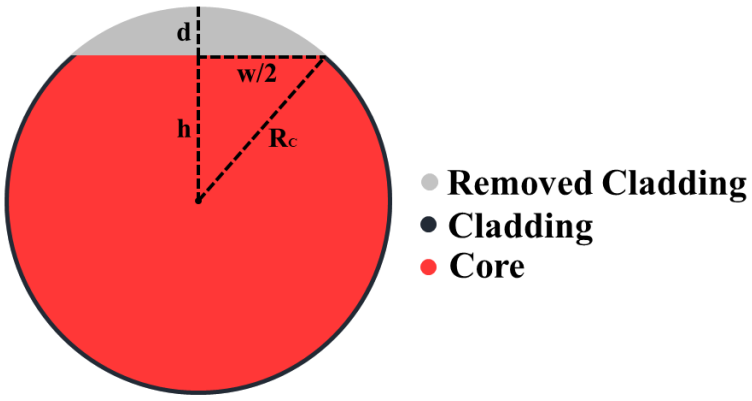

Source: Produced by the author.

In Figure 20, d represents the polishing depth, R_C the original cladding radius and w the width of the polished region. The letter h can be interpreted as the residual core thickness in POF-Ds fabrication, but for the SMF-Ds is called residual core thickness, since the removal usually stops before than reaches the core. From this model, it is possible establish the math relation:

$$R_C^2 = h^2 + \left(w/2\right)^2 \tag{14}$$

To insert d into this equation, we can use the expression:

$$h = R_C - d \tag{15}$$

where, after combining the two equations we obtain:

$$R_C^2 = (R_C - d)^2 + \left(w/2\right)^2 \rightarrow R_C^2 = \left(R_C^2 - 2R_C d + d^2\right) + \left(w/2\right)^2 \rightarrow \tag{16}$$
$$d^2 - 2R_C d + \left(w/2\right)^2 = 0$$

Using this last Equation, the estimation of the depth reached by the polishing can be summarized as the measurement of the polished region width. Aiming this measurement, the software ImageJ was used to obtain the w value from images as in Figure 19, thanks to its functionality of estimating a specific size using a known measure as a reference. The most common reference used is the width of the optical fiber that does not receive polishing.

The second step is based on the execution of measurements using materials with known refractive index values, such as distilled water, isopropyl alcohol and glycerol (glycerin). Such measurements allow for defining the operating parameters of each device or even indicating the need for some additional polishing step. The materials used are chosen considering some criteria such as non-toxicity, so that they do not represent a great increase in complexity in the construction of the sensor and, at the same time, that the characterization can be repeated whenever necessary, without major risks.

The refractive index values of the substances used in the calibration process were all obtained from works found in the literature (Rheims & Wriedt, 1997; Sani & Dell'Oro, 2016; Segelstein, 1981). The only exception found was glycerin, specifically for the wavelength of 1310 nanometers, where no studies were found in the literature that presented this result. This value, instead, was obtained from the extrapolation of the measurements for the refractive index of glycerin between 589 to 1050 nanometers (Rheims & Wriedt, 1997), using the reduced Cauchy transmission equation (Born & Wolf, 2019). This equation establishes an empirically obtained relationship between the refractive index of a transparent material and the wavelength

of the optical signal incident on it (Born & Wolf, 2019). This relationship with specific coefficients for glycerin is given by

$$n(\lambda) = 1.45797 + 0.00598 \cdot \lambda^{-2} - 0.00036 \cdot \lambda^{-4} \quad (17)$$

where n is the refractive index and λ the optical signal wavelength (Rheims & Wriedt, 1997). The values obtained from this expression can be seen in Figure 21.

Figure 21 – Graph obtained from extrapolation of the results presented by (Rheims & Wriedt, 1997).

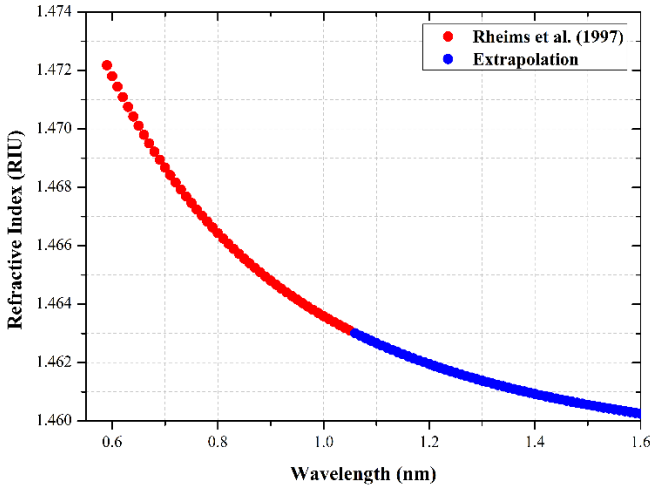

Source: Produced by the author.

As shown in Figure 21, the red dots were obtained from the original dataset, while the blue dots were the result of extrapolation using the Cauchy Equation. Once the refractive index value for glycerin was obtained, aqueous solutions of glycerin at different concentrations were also used in order to increase the number of measurements during characterization. The refractive index of these solutions varies linearly according to the concentration and this relationship is given by:

$$n_i = n_{water} + (n_{glycerin} - n_{water}) \cdot C_i \quad (18)$$

where C_i is the concentration of glycerin in the solution (in percent) and n_i, n_{water} and $n_{glycerin}$ are the refractive indices of the solution, water and pure glycerin, respectively (Teng et al., 2016). Table 4 displays all substances used and their respective refractive indices in the two wavelengths used.

Table 4 – Values of refractive indices for each substance used in characterization process.

Substance	n (λ = 650 nm)	n (λ = 1310 nm)
Distilled Water	1.3307	1.3217
Isopropyl Alcohol	1.3758	1.3686
Glycerin (50%)	1.4004	1.3915
Glycerin (75%)	1.4353	1.4264
Glycerin (90%)	1.4562	1.4473
Glycerin (95%)	1.4631	1.4543
Glycerin (100%)	1.4701	1.4613

Source: Produced by the author.

Finally, to ensure a consistent characterization process, a well-defined routine was determined, ensuring the execution of each of the measurements as uniformly as possible. This routine is detailed in Figure 22 and helps to illustrate how simple this process of using the sensor is, validating the use of the device as a simple fabrication, operating and maintenance solution.

Figure 22 – Block diagram used to guide the calibration process and, posteriorly, the measurement process.

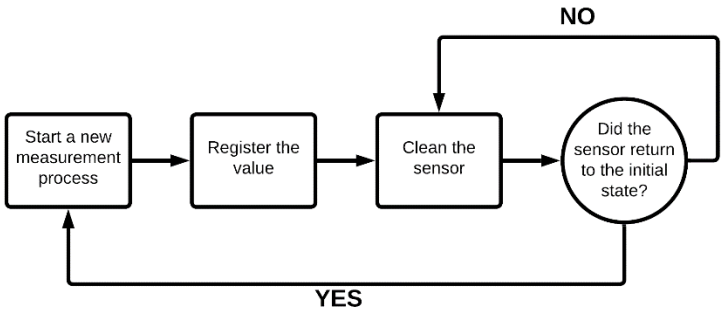

Source: Produced by the author.

3.5. EXPERIMENTAL SETUP USED IN MEASUREMENTS

The standard setup used in carrying out the experimental measurements is composed of the same light source and OPM used during the fabrication process. Figure 23 illustrates this setup. Another similarity with the methodology used during the manufacture of the devices is that the process essentially consists of measuring in real time the level of optical power transmitted by the optical fiber.

Figure 23 – Representation in block diagram of the setup used to characterize the produced sensors and perform the measures.

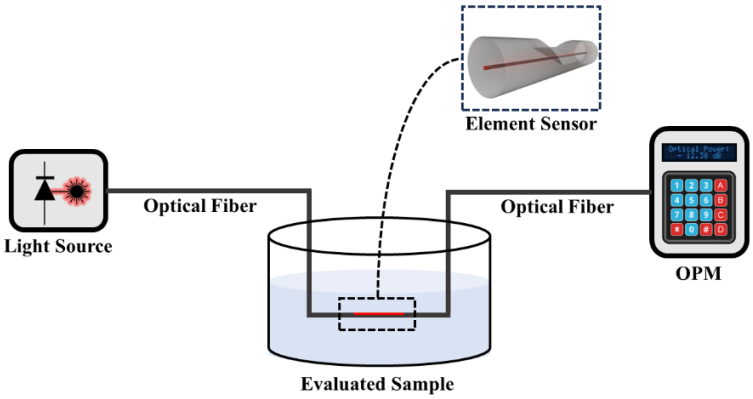

Source: Produced by the author.

The setup in Figure 23 was used throughout the optical fiber characterization process and the other measurements with one exception: the use of SMF-Ds in the construction of a multipoint sensor for detecting leaks or oil spills. In this specific case, an infrastructure was built to simulate the installation of devices in pipelines that are essential elements in the flow of production in the oil and gas sector. In this context, the efficient management of these structures can be the difference between a productive operation or a large-scale environmental disaster with profound socioeconomic impacts.

For the construction of this device, two SMF-Ds were used in series composing a single link, configuring a multipoint device without the necessity of isolators or splitters. Figure 24 shows this setup. In addition, the optical fibers used were fabricated according to some parameters such as a low level of roughness and a common optical insertion loss. The low level of roughness is intended to facilitate the sensor's self-cleaning process and mitigate sensor element inactivation due to persistent oil adhesion. In parallel, the low optical loss allows the use of several sensor elements in the same link, opening space for new explorations in future works.

Figure 24 – Setup used to simulate leak detection in a pipeline.

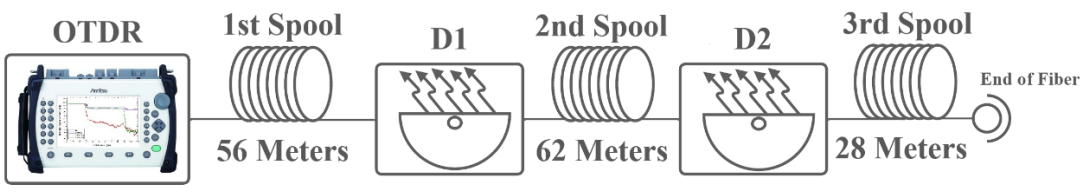

Source: (Barros et al., 2022b).

As shown in Figure 17, the link with the SMF-Ds was coupled to a commercial optical time domain reflectometer (OTDR). This device sends optical signals in the form of pulses in an optical fiber and evaluates the amplitude and period of the returned signal due to reflections or scattering (Peixoto E Silva et al., 2021). Based on the analysis of these pulses, this device spatially locates sources of reflections/scattering (Peixoto E Silva et al., 2021). This technique is called optical time domain reflectometry and is widely used in the characterization of optical links. As mentioned before, it is also used in multipoint or distributed optical sensors, such as distributed temperature sensors.

In addition, it is worth mentioning that as the OTDR evaluates the reflected and not transmitted signal, the configuration used until then, with a photodetector at the end of the link, becomes unnecessary. Although it seems simple, this observation is important, since the presence of photodetectors at the end of the link can result in a significant increase in cost and complexity, since, in addition to the pipelines being kilometers long, they are commonly located in inaccessible regions.

Still according to Figure 24, it is also possible to observe the inclusion of optical fiber spools. The first of these spools was inserted in order to avoid the region known as the dead zone, where the commercial OTDR cannot perform measurements. The second and third spools were inserted in order to distance the SMF-Ds from each other and from the end of the fiber, respectively. This distancing does not necessarily reflect a limitation of the system, given that the spatial resolution of the OTDR is around 1 meter, but they contribute to a more accurate simulation of the desired scenario, where the sensor elements will possibly be distanced by tens of meters.

4 COMPUTATIONAL MODEL RESPONSE

The first results obtained after the fabrication process were those referring to the computational modeling of the D-shaped optical fibers. The importance of these results lies in the ability to use them to verify the sensor's response even during the measurement process. Through them it is possible not only to diagnose possible discrepancies, but also to identify the validity of the theoretical model through the repetition of measurements.

The simulation of the models using COMSOL Multiphysics was performed by varying the optical parameters of the domain referring to the external environment. Having the refractive index as the central parameter, this parameter was varied according to the values established in the literature for the substances used in the calibration stage. The consonance in choosing these values is a key point to evaluate the sensors produced and, consequently, the entire fabrication process. The answers obtained in this step are shown in Figure 25.

Figure 25 – Responses obtained from the computational models. The SMF-D response is represented in the left graph, while the POF-D response can be visualized in the right graph.

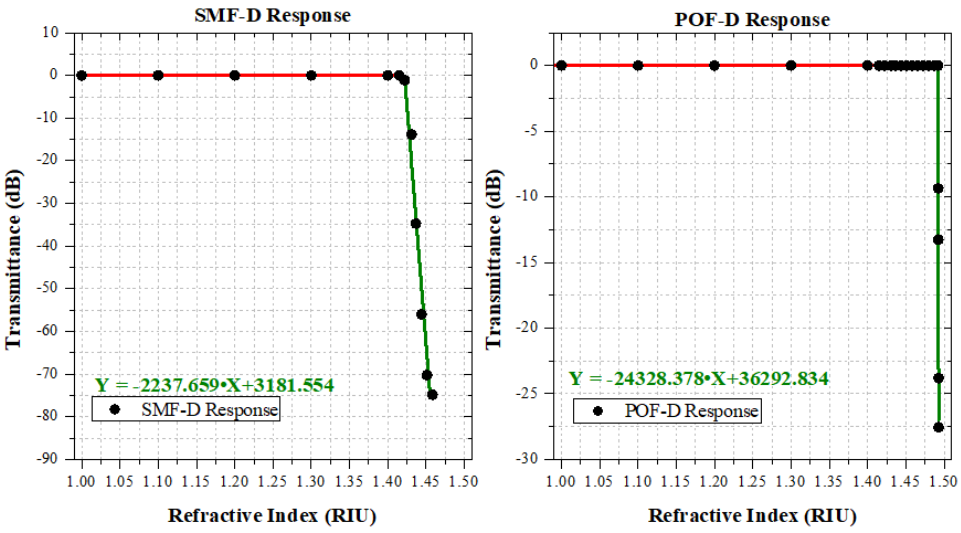

Source: Produced by the author.

From Figure 25 it is possible to distinguish two possible regions of operations. The transition region between these two operating ranges occurs close to a critical value slightly lower than the refractive index of the optical fiber core. This value corresponds to the effective index of refraction of the propagation mode, obtained by COMSOL from the optical and geometric parameters of the simulation.

The alternation of behavior between the two operating regions can be described as a direct consequence of breaking the necessary conditions for the occurrence of multiple total internal reflections (Alves, 2020; Born; Wolf, 2019). This break occurs for refractive indices equal to or greater than the effective refractive index value of the structure corresponding to the D-shaped (Alves, 2020). In this scenario, the core of the optical fibers becomes the least refractive medium, resulting in the optical signal escaping to the external medium (Alves, 2020). Also from Figure 25, it is possible to observe that the sensors do not respond to variations in the refractive index of the external environment during this first operating range. This behavior, which seems to make the use of these devices unfeasible in sensing media with a refractive index smaller than the effective refractive index, is only changed for values greater than this critical value.

Since in the second operating range a small increase in the refractive index results in a large loss of optical power, it is possible to associate a large sensitivity value to these devices. This sensitivity can be obtained through the slope of the straight line that describes the response of each sensor in this range. The module values obtained were 2237.659 dB/RIU for the SMF-D sensor and 2424.328 dB/RIU for the POF-D sensor.

The first experimental results obtained were within the context of fuel adulteration, as no additional components were required for this configuration. The experiments were carried out on two sets of measurements, each of which was carried out using optical fiber technology. All fuel samples were provided by the Fuel Analysis Laboratory (LAC-LITPEG) at the Federal University of Pernambuco. Measurements were performed at a constant temperature, aiming to mitigate the effects of temperature on the analyzed optical parameters. In particular, measurements with fuels were carried out in a hood with support for gas exhaustion, together with the use of appropriate personal protective equipment.

5 FUEL ADULTERATION SENSORS

This chapter presents the results obtained using the proposed sensor as a detector of fuel adulteration. In Section 5.1, the results obtained from measures using samples of diesel adulterated with kerosene are described. The Section 5.2 presents the implementation of the proposed sensor as a solution to detect the water content in fuel ethanol, allowing the use of the device beyond the adulteration detection, but exploring the quality control. Finally, Section 5.3 closes the chapter by exploring measures with gasoline adulterated with ethanol.

5.1. DETECTION OF DIESEL ADULTERATION

The first scenario explored was the adulteration of diesel through the addition of kerosene. Bearing in mind that both have high refractive indices in relation to the limiting value for the SMF-D operating regions, this technology was used in order to explore its second operating range. This choice allowed measurements to be taken in a region of greater sensitivity, allowing solid results to be obtained even within a narrow range of values for the refractive indices (about 0.002 RIU). This measurement is shown in Figure 26.

Figure 26 – Values obtained from measurements with diesel mixtures, highlighting the linear fit and its equation, both represented in red.

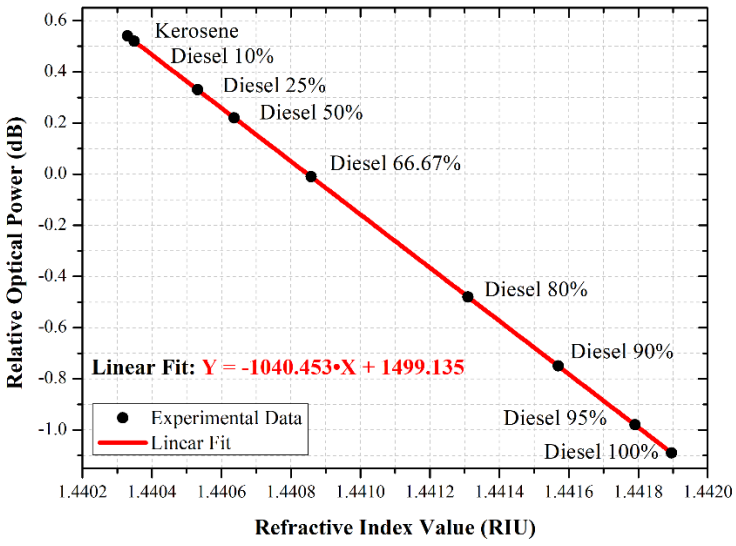

Source: (Barros et al., 2023c).

Similar to what was previously discussed, the sensitivity of the device produced can be determined through the slope of the linear fit, represented in red in Figure 26. The value

obtained for this sensitivity is 1040.453 dB/RIU, which indicates the device's resolution to detect variations related to the refractive index of the order of 10^{-6} RIU. This resolution was determined considering the OPM resolution of 0.01 dB, through the expression:

$$R_{Sensor} = \frac{R_{OPM}}{S_{Sensor}} \tag{19}$$

where R_{Sensor} and R_{OPM} represent the sensor and the OPM resolution, respectively. S_{Sensor} in turn corresponds to the sensor sensitivity determined by the slope of the linearization. Still, in Figure 26, it is possible to observe the non-uniformity in the distribution of the points on the line in red, indicating a non-linearity between the concentration of kerosene in the diesel and the corresponding relative optical power values. The Graph shown in Figure 27 shows this relationship in more detail.

Figure 27 – Relative transmitted optical power as a function of kerosene concentration in diesel, representing the sensor response to diesel adulteration.

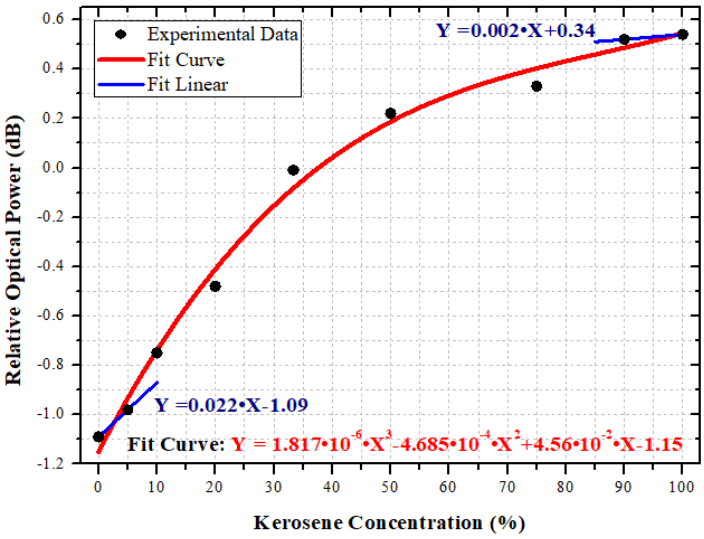

Source: (Barros et al., 2023c).

This relationship is nonlinear and can be approximated by the cubic function shown in Figure 27 with a correlation coefficient of 0.9967. Using this function is possible to estimate the sensitivity of the sensor for low concentrations of kerosene in diesel (5%) and for high concentrations of kerosene in diesel (90%). These are particularly interesting ranges that simulate, respectively, the addition of kerosene to increase fuel volume and the replacement of diesel with kerosene. Similar to how the sensitivity was obtained in the graph of Figure 26, it

can be determined through the angular coefficient of the line equations that passes through the points of interest. These angular coefficients are given by

$$\alpha = \frac{Y_B - Y_A}{X_B - X_A} \tag{20}$$

where X and Y correspond to the points coordinates in ordered pair form (X, Y), α represents the angular coefficient and the subscripts indicate the points used according to Table 5.

Table 5 – Values used in determination of the sensitivity for mixtures containing 5% and 90% of kerosene.

Operating Range	**Point A (X_A,Y_A)**	**Point B (X_B,Y_B)**	**Correspondent Sensitivity**
5%	(0, -1.09)	(5, -0.98)	0.022 dB/%
90%	(90, 0.52)	(100, 0.54)	0.002 dB/%

Source: (Barros et al., 2023c).

This high value of sensitivity and resolution corroborates with the initial expectations that motivated the choice of the SMF-D as an element sensor for the detection of adulterations in a medium as refringent as diesel. This behavior was intensified thanks to deep polishing performed during the fabrication process. From there, this SMF-D has a residual cladding of 1.97 μm and a length of 13 mm.

5.2. DETECTION OF ETHANOL ADULTERATION

In addition to the adulteration of diesel with kerosene, the adulteration of ethanol with water was also explored. In this second scenario, a similar methodology was used, but with the replacement of a SMF-D by a POF-D. This change was made because, given the values obtained in the literature for the refractive index of distilled water and ethanol, it is expected that all measurements occur in the range corresponding to the first region of operation for both optical fiber technologies. This expectation was confirmed as shown in Figure 28. As already presented and evidenced by the response obtained from the computational model, this operating range is less sensitive and increases the relevance of criteria, such as the greater mechanical resistance, favoring the plastic optical fibers.

Figure 28 – Values obtained from measurements with ethanol mixtures, highlighting the linear fit and its equation, both represented in red.

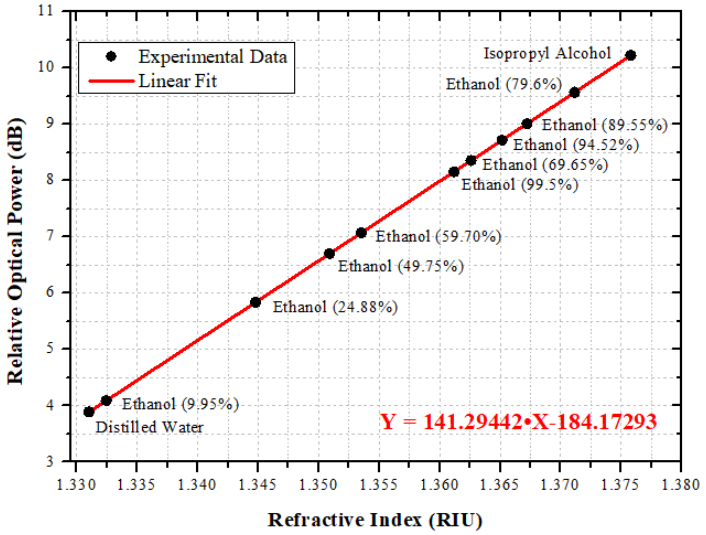

Source: (Barros et al., 2023d).

Similar to what was done with the SMF-D sensor in diesel adulteration, the sensitivity of the sensor produced can be determined through the slope of the linear fit that approximates the device response, represented in red in Figure 28. The sensitivity value of 141.294 dB/RIU corresponds to the resolution value of $7.077 \cdot 10^{-5}$ RIU, according the methodology applied in Section 5.1. This POF-D was fabricated with a length of 13 millimeters and the depth reached at the end of polishing was 292.51 μm.

Furthermore, in direct comparison with the result shown in Figure 26, it is possible to observe a fundamentally different behavior for ethanol samples in relation to diesel samples. As already discussed, although the non-linearity implies the non-uniform distribution of the points on the linearization, these points occur on the line in an ordered manner, showing that the refractive index progressively decreases as more kerosene is added to the total volume of the sample. In the case of ethanol, this behavior does not happen and can be more easily visualized through the curve shown in Figure 29.

The behavior shown in Figure 29 is well described in the literature and occurs due to molecular interactions between water and ethanol (Srivastava et al., 2011). For small concentrations of water in ethanol, these interactions favor the formation of clusters that increase the refractive index of the solution (Srivastava et al., 2011). As the water concentration increases, this effect ceases and the general behavior of the refractive index becomes similar to that of the diesel-kerosene mixture.

Figure 29 – Relationship between the value of the refractive index and the concentration of water in an aqueous solution of ethanol.

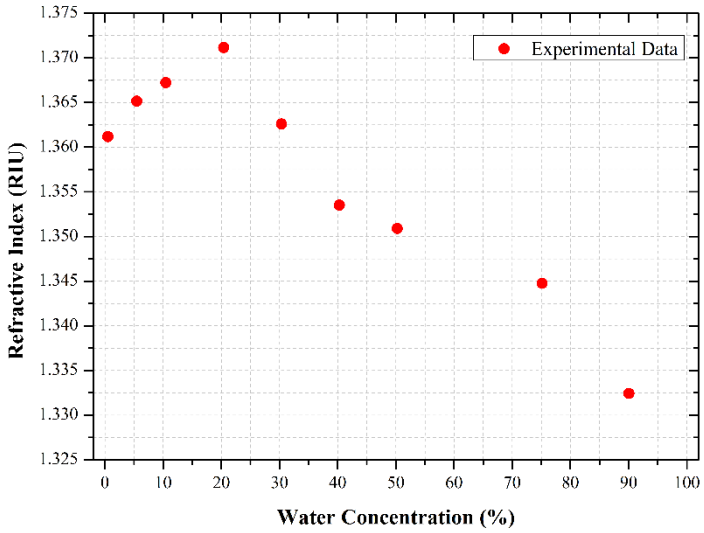

Source: (Barros et al., 2023d).

Finding the behavior shown in Figure 29 brings with it an important consideration about the methodology used in the measurement process. Direct measurement of the refractive index value as a way of detecting possible adulterations may be unfeasible, given that the observed curve results in the same power value for two different concentrations. Even so, this apparent limitation can be dodged by measuring the displacement of the refractive index by the controlled addition of water during the measurement.

The methodology mentioned above, although not ideal, can be easily standardized and reproduced in the field, making it a viable option since alternative methods may involve significantly more complex sensors (Srivastava et al., 2011) or more expensive methods (H. E. Bezerra et al., 2001). Furthermore, from the point of view of the production process, the concentrations of water obtained during ethanol production are typically less than 10% (Meirelles et al., 1992), bypassing this possible limitation and making the proposed device an interesting solution to be integrated into the production process.

5.3. DETECTION OF GASOLINE ADULTERATION

Similar to the adulteration of ethanol using water, preliminary measures have shown the feasibility of using POF-Ds to detect adulteration of gasoline. In this new scenario, the adulterant used is ethanol, in view of its lower cost and the existence of a pre-existing volume of ethanol in commercialized gasoline. The measurements are shown in Figure 30.

Figure 30 – Values obtained from measurements with gasoline mixtures, highlighting the linear fit and its equation, both represented in red.

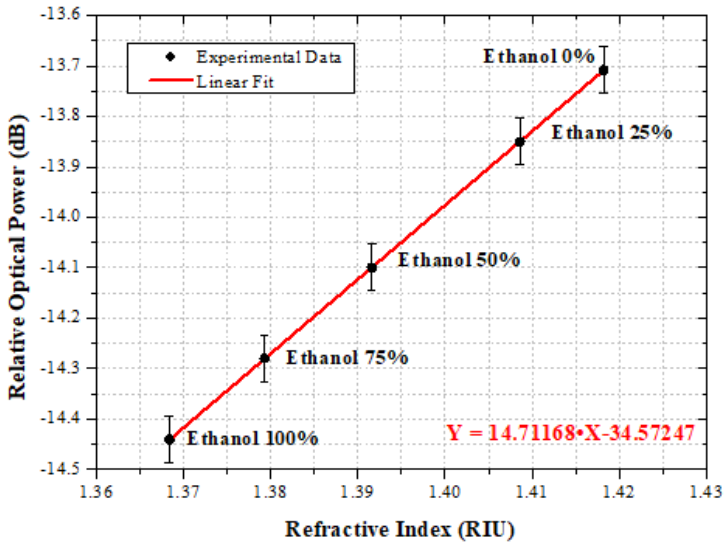

Source: (Barros et al., 2022).

Once again, it is possible to obtain the sensitivity of the sensor built from the slope of the line shown in Figure 30. From this value (14.712 dB/RIU), it is also possible to determine the resolution, using the same expressions presented in Section 5.1, obtaining a value of $6.797 \cdot 10^{-4}$ RIU. This difference between the sensitivity and resolution of the system during measurements with ethanol-water and gasoline-ethanol can be explained by the difference in depth reached during the manufacturing process. For this second optical fiber, the polishing was more superficial reaching a depth of 236.61 μm.

Still on Figure 30, important considerations must be made. The first of them refers to the initial alcohol content in the gasoline, which was not considered, since the initial purpose of the measurement was to evaluate the effect of adding ethanol in a commercial sample on the value of the refractive index. The methodology used to determine this initial value is still under development, in order to ensure the effectiveness of the method, as well as the safety of the process. Another important consideration that can be confirmed by Figure 30 is the apparently similar relationship to the result obtained in diesel adulteration (Figure 26). This is an expected result due to the composition of gasoline: mostly non-polar hydrocarbons. This non-polarity does not foster relationships as seen in the addition of small concentrations of water to ethanol.

6 DISTRIBUTED MULTIPOINT OIL DETECTOR

The first result obtained for the multipoint system proposed and described in Section 3.5 is a simple response test to verify the operation of each SMF-D. Figure 31 shows the sensor response during these measurements.

Figure 31 – Response of the two SMF-Ds that make up the multipoint sensor.

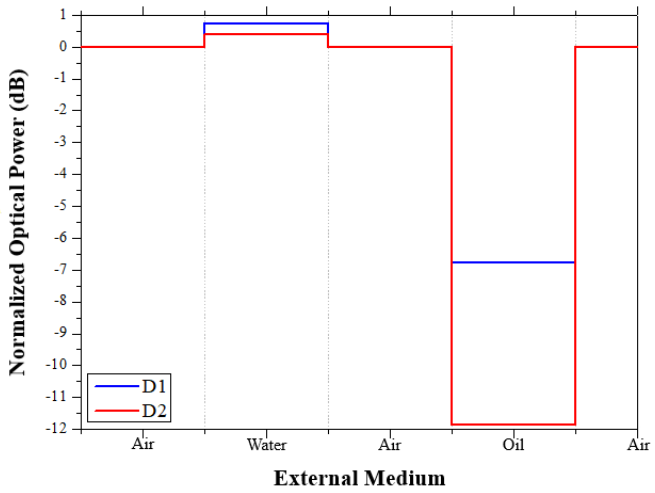

Source: (Barros et al., 2023b).

Through the responses shown in Figure 31, it is possible not only to attest to the functioning of the system but also to conclude some important information regarding the SMF-Ds produced. The first of these conclusions can be made taking into account the small difference between the two sensors while submerged in water. This variation, although small, can be associated with a difference in the level of roughness of the polished surfaces of the devices (Alves et al., 2022), resulting in a greater gain for the one with greater roughness (D1). This type of analysis is commonly used to verify the ability of the proposed system to perform polishing with a certain degree of constancy.

The second type of information that can be obtained from the graph in Figure 31 is the difference in terms of the optical power of the sensors when in contact with the crude oil. In this case, the greater optical power variation in the transition from air to oil may indicate a deeper polishing in D2 than D1 or, in a complementary way, that D2 has a smaller residual cladding thickness, about 1.41 μm, while D1 has 4.8 μm of residual cladding.

After the tests, measurements began using reflectometry, as shown in Figure 32. Four measurements were performed, the first of which was in the air, the second with the system submerged in water, and the third and fourth with the sensors in contact with the oil.

Figure 32 – Superposition of measurements obtained by optical time domain reflectometry highlighting the spatial coordinates of D1 and D2, marked on the horizontal axis. Dashed lines indicate the initial level of emitted optical power used as references.

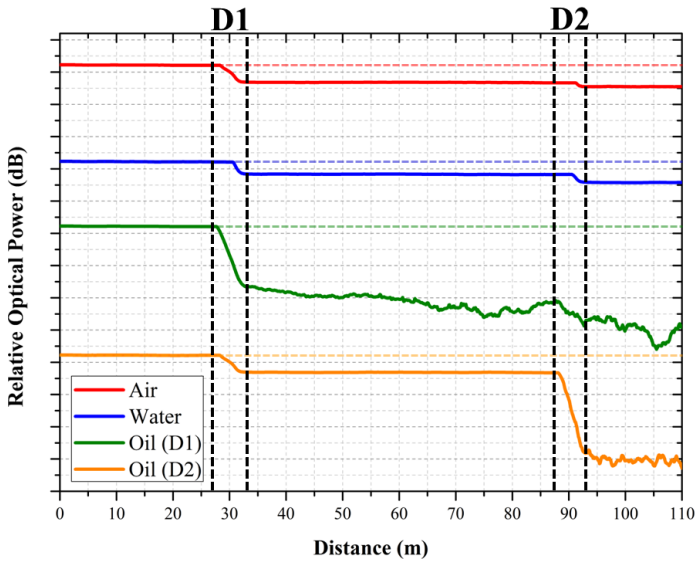

Source: (Barros et al., 2023b).

From Figure 32 it is possible to observe that the system is able to locate the sensor elements and clearly distinguish the presence of oil or some other material with a high refractive index value. It is also important to mention that the proposed system is the first version of a multipoint digital system, so it is only intended to detect and locate the presence of oil, without any additional intentions that imply intermediate measures. It is also possible to observe that the high sensitivity of the optical fibers produced can limit detection by multiple sensor elements. Alternative strategies to reduce this sensitivity have been tested, such as the fabrication of OF-Ds with smooth surface and shorter sensor elements. Based on all this discussion, Figure 33 shows possible applications for the proposed sensor.

Figure 33 – Representation of the proposed sensor installed on a pipeline (a) and as a level sensor to reservoir management (b). In both cases, dimensions out of scale.

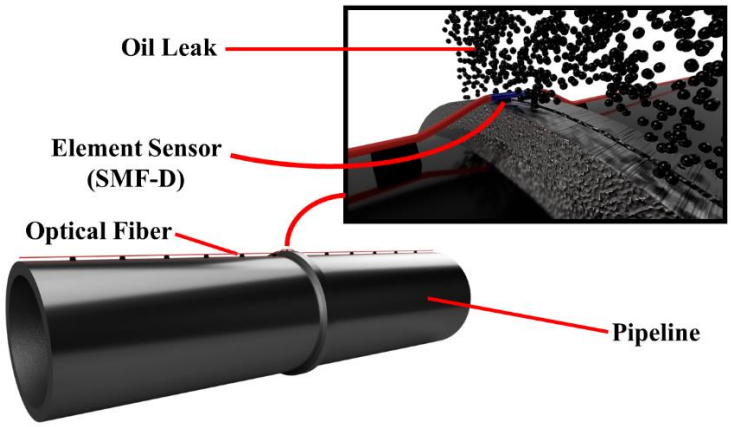

(a)

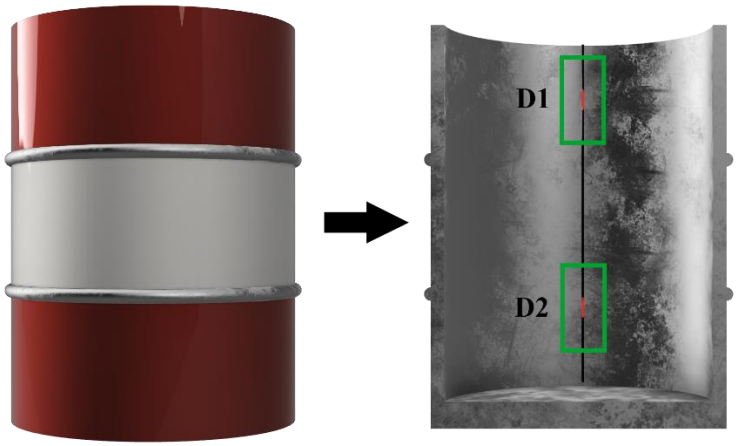

(b)

Source: (Barros et al., 2022b).

As shown in Figure 33(a), the concept behind the use of the proposed device is to install it so that the sensor elements are located in points more susceptible to corrosion or mechanical damage, such as in joints or in large curvatures. The application as a reservoir level sensor, illustrated in Figure 33(b), although conceptually simple, is extremely important within the context of the oil and gas industry, in addition to having the differential that it is a sensor capable of differentiate the stored substances.

7 FERTILIZER CONCENTRATION SENSOR

As mentioned in Section 3.3, before obtaining the response of the proposed device, the influence of geometric parameters on the response of the modeled sensor was explored. These two parameters were the residual cladding thickness (d) and the length of the D-shaped region (L). Figure 34 shows the responses obtained by changing each of these parameters.

Figure 34 – Sensor responses considering different length of the D-shaped region with d = 1.5μm (a) and different residual cladding width with L = 20μm (b).

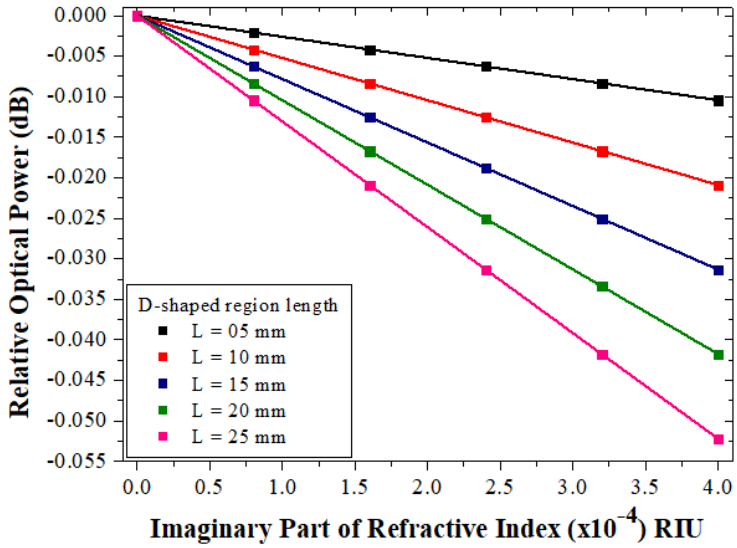

(a)

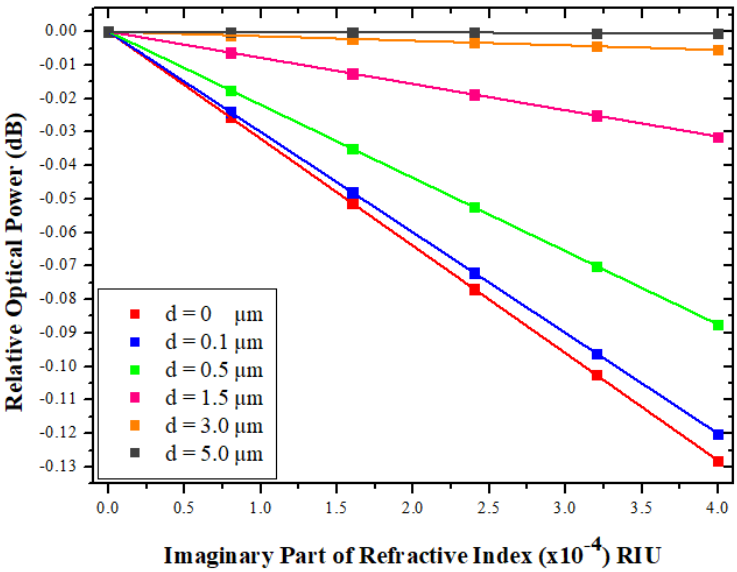

(b)

Source: (De Barros et al., 2022b).

According to the Figure 34, it is possible to verify that although both parameters influence the device's response, this influence occurs in different ways. While in Figure 34(a) a uniform increase in the sensitivity of the devices is seen as L increases, in Figure 34(b) it is seen that the thickness of the residual cladding has a more significant contribution as d approaches zero. All this behavior can be observed directly through the behavior of the slopes of the linearization shown in Figure 34, since, as already discussed, they correspond to the sensitivity of the device.

In view of the results obtained, a SMF-D without residual cladding and with a length L = 25 mm was modeled. Although the general idea is to maximize the sensitivity of the device, a size greater than 25 mm was not adopted in this study in view of the practical feasibility of fabrication such a device, since it is the maximum size ever experimentally produced. The response obtained is shown in Figure 35.

Figure 35 – Sensor response in aqueous solutions with different concentrations of dissociated nitrate or sulfate.

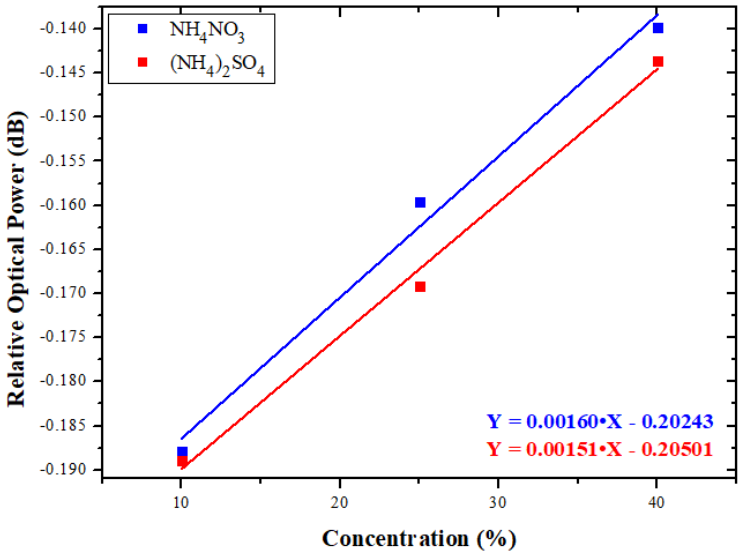

Source: (De Barros et al., 2022b).

According to Figure 35, it is possible to observe that the sensor presented a sensitivity of 0.00160 dB/% for ammonium nitrate and 0.00151 dB/% for ammonium sulfate. Although this is an initial study, this result guides the next steps in the search for an operational device and serves as a basis for exploring new possibilities such as the use of Surface Plasmon Resonance (SPR) or other phenomena to enhance the response and increase the degree of selectivity of the sensor.

8 CONCLUSIONS

This chapter summarizes the main contributions obtained from the results presented in this dissertation while listing the future perspectives related to obtaining these results.

8.1. STUDY CONTRIBUTIONS

This work presents the characterization and fabrication process of D-shaped optical fiber sensors. Two different optical fiber technologies were used: single-mode optical fiber and plastic optical fiber. As a way of guiding the fabrication and characterization process, this work also presented the development of a computational model, where the COMSOL Multiphysics software was used to obtain the simulation results for the responses of the proposed devices.

Differences between simulation and experimental results were explored to complement discussions on important device parameters such as the level of roughness of the polished surface and the thickness of the residual cladding. These parameters were also addressed according to the functionality proposed to the device to optimize its operation.

Different problems faced by the oil and gas industry were explored, such as fuel adulteration and oil leakage in pipelines. Both optical fiber technologies were used in the detection of fuel adulteration, allowing the evaluation of the response of each system and verifying that although plastic optical fibers present greater robustness due to their size, systems based on silica optical fibers presented a greater sensitivity.

Using a sensor based on SMF-D, measurements were performed in order to verify the sensor's ability to characterize mixtures of diesel and kerosene. Kerosene was chosen because it is a common adulterant for this type of fuel. The length of the manufactured SMF-D was 13 mm and the residual cladding thickness after polishing was 1.97 μm. The sensitivity for this system was 1040.453 dB/RIU, resulting in a resolution of the order of 10^{-6} RIU.

Specifically in the context of ethanol, two types of experiments were carried out. The first involved the adulteration of ethanol by adding water. Given the ease of carrying out this adulteration, added to the difficulty in detecting it, since both substances are mostly transparent, the importance of the presented results is emphasized. In addition, as the addition of water can be performed accidentally due to the natural formation of water during ethanol refining, the proposed device also presents itself as a potential solution for quality control in refineries and alike. For this first experiment, a POF-D with 13 mm in length and polished depth of 292.51

μm was used as the sensor element. The system presented a sensitivity of 141.294 dB/RIU and a resolution of $7.077 \cdot 10^{-5}$ RIU.

The second scenario involving ethanol that was explored consisted of gasoline adulteration using ethanol as an adulterant. In this case, a POF-D with a length of 13 mm and a polished depth of 236.61 μm was used. Possibly because of this lower depth, the system had a lower sensitivity compared to the previous system used in ethanol-water mixtures. The obtained sensitivity was 14.712 dB/RIU, resulting in a resolution of $6.797 \cdot 10^{-4}$ RIU which, although smaller, is sufficiently high to detect samples that present a higher ethanol content than that determined in Brazilian legislation.

In the context of detecting oil leaks in pipelines, a measurement system based on a commercial optical time domain reflectometer was developed. This device allows the spatial location of the sensor elements, allowing not only to discriminate which sensor detected the leak but also to assess the radius and propagation speed in the event of a spill. In contrast to other systems with similar proposals in the literature, this device was built exclusively from two SMF-D sensors in series, without splitters, insulators or any other optical devices.

In addition to the simplified structure, the sensor has a total length of 110 meters, with a spatial resolution of approximately 1 meter. Moreover, the multipoint system also proved to be able to detect water and, consequently, other fluids with a lower refractive index. This capacity, together with the resolution obtained, enables its use in other applications not necessarily linked to oil, such as level measurement in reservoirs.

Finally, this work also explored the computational model initially built in order to guide the fabrication process of D-shaped optical fibers. In view of the current context of energy transition and the progressive increase in biofuel production from plants such as sugar cane or corn, the use of SMF-D was proposed as a solution to enable more efficient management of fertilizer use. For this purpose, SMF-D was used as an absorptiometer for the detection of nitrate and sulfate ions, where these ions were chosen due to their importance in the plant absorption of nitrogen and sulfur. From this study, the influences of geometric parameters such as polishing depth on the final response of the device were also evaluated, helping in the optimization of the fabrication process of D-shaped optical fibers.

8.2. FUTURE PERSPECTIVES

From all the results that were presented, some important points of improvement can be established in order to circumvent possible limitations. The first of these possible improvements

is to change the geometric parameters of the produced SMF-Ds in order to reduce sensitivity and insertion loss. This change should allow an increase in the number of sensor elements that make up the link used with the OTDR to detect oil leaks.

From the point of view of fuel adulteration, it is expected to explore new scenarios such as the use of other adulterants. Especially in the case of gasoline adulteration through the addition of ethanol, it is expected to carry out new measures in addition to developing an appropriate methodology capable of extracting the ethanol present in gasoline, since obtaining ethanol-free gasoline is prohibited by Brazilian regulations. Due to the high sensitivity of the devices when used as detectors of substances with high refractive indexes, such as oils. This work also enabled the construction of devices to interrogate food oils to detect possible adulterations. Finally, it is also expected to improve and fabricate a SMF-D sensor to sense the concentration of nitrate and sulfate ions, given their importance in managing the use of fertilizers.

REFERENCES

AGRAWAL, G. P. **Nonlinear Fiber Optics**. 6. ed. [s.l.] Mara Conner, 2019.

ALKAZIMI, M. A.; GRANTHAM, K. Investigating new risk reduction and mitigation in the oil and gas industry. **Journal of Loss Prevention in the Process Industries**, v. 34, p. 196–208, 12 fev. 2015.

ALVES, H. P. **Fibra óptica com perfil D : fabricação e aplicações em sensoriamento**. Recife: Federal University of Pernambuco, 18 dez. 2020.

ALVES, H. P. et al. Influence of surface roughness on the sensitivity of a D-shaped optical fiber-based refractive index sensor. **Sensors and Actuators A: Physical**, v. 344, 1 set. 2022.

ASHRY, I. et al. **A Review of Distributed Fiber-Optic Sensing in the Oil and Gas Industry**. **Journal of Lightwave Technology**Institute of Electrical and Electronics Engineers Inc., 1 mar. 2022.

AVAGO. **HFBR-0507Z Series HFBR-15X7Z Transmitters HFBR-25X6Z Receivers Datasheet**. Avago Technologies, , 11 abr. 2012.

BADMOS, A. Y.; AJIMOTOKAN, H. A.; EMMANUEL, E. O. **Corrosion in Petroleum PipelinesNew York Science Journal**. [s.l: s.n.]. Disponível em: <http://www.sciencepub.net/>.

BARROS, T. H. C. et al. **D-Shaped Plastic Optical Fibers: Fabrication and Characterization as Refractive Index Sensor**. 2021 SBMO/IEEE MTT-S International Microwave and Optoelectronics Conference (IMOC). **Anais**...Fortaleza: 2021.

BARROS, T. H. C. et al. **Computational Modeling of D-shaped Optical Fiber Nitrate and Sulfate Sensor**. SBFoton IOPC 2022 - SBFoton International Optics and Photonics Conference. **Anais**...Recife: Institute of Electrical and Electronics Engineers Inc., 2022a.

BARROS, T. H. C. et al. **D-shaped Optical Fiber Refractive Index Sensor for Application in Fuel Oil Mixtures and Leakage Detection**. Proceedings of the Rio Oil & Gas Expo and Conference. **Anais**...Rio de Janeiro: Brazilian Petroleums and Gas Institute - IBP, nov. 2022b.

BARROS, T. H. C. et al. **D-shaped Optical Fiber Refractive Index Sensor for Application in Fuel Oil Mixtures and Leakage Detection**. Proceedings of the Rio Oil & Gas Expo and Conference. **Anais**...Rio de Janeiro: Brazilian Petroleums and Gas Institute - IBP, nov. 2022c.

BARROS, T. H. C. et al. **Thermal Influence on Plastic Optical Fibers: A Reliability Study**. Proceedings of the 33rd European Safety and Reliability Conference (ESREL 2023). **Anais**...Singapore: Research Publishing, 2023a.

BARROS, T. H. C. et al. **Multipoint sensor based on D-shaped optical fiber for detection of leaks in pipelines**. Proceedings of the Rio Pipeline Conference & Exhibition. **Anais**...Rio de Janeiro: Brazilian Petroleum and Gas Institute - IBP, 28 fev. 2023b. Disponível em: <https://doi.org/10.48072/2447-2069.rpc.2023.>. Acesso em: 14 ago. 2023

BARROS, T. H. C. et al. **Diesel Adulteration Sensor Based on D-Shaped Optical Fiber**. 2023 SBMO/IEEE MTT-S International Microwave and Optoelectronics Conference (IMOC). **Anais**… Barcelona: 2023c.

BARROS, T. H. C. et al. **D-shaped Plastic Optical Fiber Sensor for Detection of Ethanol Fuel Adulteration**. 2023 International Conference on Optical MEMS and Nanophotonics (OMN) and SBFoton International Optics and Photonics Conference (SBFoton IOPC). **Anais**… Campinas: 2023d.

BEZERRA, A. C. DE M. et al. Quantification of anhydrous ethanol and detection of adulterants in commercial Brazilian gasoline by Raman spectroscopy. **Instrumentation Science and Technology**, v. 47, n. 1, p. 90–106, 2 jan. 2019.

BEZERRA, H. E.; SILVA, D. A.; PASQUINI, C. **Dual-Beam Near-Infrared Hadamard Spectrophotometer APPLIED SPECTROSCOPY**. [s.l: s.n.].

BOAZ, L.; KAIJAGE, S.; SINDE, R. An overview of pipeline leak detection and location systems. 2014.

BOLOGNA-CAMPBELL, I. et al. Impact of Nitrogen and Sulphur Fertilisers on Yield and Quality of Sugarcane Plant Crop. **Sugar Tech**, v. 15, n. 4, p. 424–428, dez. 2013.

BONNAUD, C. et al. Experimental study and modelling of the consequences of small leaks on buried transmission gas pipeline. **Journal of Loss Prevention in the Process Industries**, v. 55, p. 303–312, 1 set. 2018.

BORN, M.; WOLF, E. **Principles of Optics**. 7th. ed. Cambridge: Cambridge University Press, 2019.

BRANDÃO, L. F. P.; BRAGA, J. W. B.; SUAREZ, P. A. Z. Determination of vegetable oils and fats adulterants in diesel oil by high performance liquid chromatography and multivariate methods. **Journal of Chromatography A**, v. 1225, p. 150–157, 17 fev. 2012.

BRÜCKNER, V. To the use of Sellmeier formula. **Senior Experten Service (SES) Bonn and HfT Leipzig**, v. 42, p. 242–250, 2011.

CABRAL, T. D. et al. Pipeline Bonded Joints Assembly and Operation Health Monitoring with Embedded FBG Sensors †. **Engineering Proceedings**, v. 2, n. 1, 2020.

CHENG, L. K. et al. **Development of a FBG vortex flow sensor for high-temperature applications**. 21st International Conference on Optical Fiber Sensors. **Anais**...SPIE, 15 maio 2011.

CIHAT ONAT, N. et al. From sustainability assessment to sustainability management for policy development: The case for electric vehicles. **Energy Conversion and Management**, v. 216, 15 jul. 2020.

CORDES, E. E. et al. **Environmental impacts of the deep-water oil and gas industry: A review to guide management strategies**. **Frontiers in Environmental Science,** Frontiers Media S.A., 16 set. 2016.

CORGOZINHO, C. N. C.; PASA, V. M. D.; BARBEIRA, P. J. S. Determination of residual oil in diesel oil by spectrofluorimetric and chemometric analysis. **Talanta**, v. 76, n. 2, p. 479–484, 15 jul. 2008.

CUNHA, D. A. et al. NMR in the time domain: A new methodology to detect adulteration of diesel oil with kerosene. **Fuel**, v. 166, p. 79–85, 15 fev. 2016.

DE BARROS, T. H. C. et al. **Computational Modeling of D-shaped Optical Fiber Nitrate and Sulfate Sensor**. SBFoton IOPC 2022 - SBFoton International Optics and Photonics Conference. **Anais**...Institute of Electrical and Electronics Engineers Inc., 2022.

DE PAULO, J. M. et al. A study of adulteration in gasoline samples using flame emission spectroscopy and chemometrics tools. **Analyst**, v. 137, n. 24, p. 5919–5924, 21 dez. 2012.

DE SOUSA, C. A.; ROMERO, O. J. Influence of oil leakage in the pressure and flow rate behaviors in pipeline. **Latin American Journal of Energy Research**, v. 4, n. 1, p. 17–29, 27 ago. 2017.

DONTHU, N. et al. How to conduct a bibliometric analysis: An overview and guidelines. **Journal of Business Research**, v. 133, p. 285–296, 1 set. 2021.

EDOUARD, M. N. et al. Application of fiber optics in oil and gas field development—a review. **Arabian Journal of Geosciences**, v. 15, n. 6, mar. 2022.

FERREIRO-GONZÁLEZ, M. et al. New headspace-mass spectrometry method for the discrimination of commercial gasoline samples with different research octane numbers. **Energy and Fuels**, v. 28, n. 10, p. 6249–6254, 16 out. 2014.

FINLEY, M. The oil market to 2030-implications for investment and policy. **Economics of Energy and Environmental Policy**, v. 1, n. 1, p. 25–36, 2012.

FONTANA, E. **Tratado de Eletromagnetismo**. 1. ed. Campinas: Editora da Unicamp, 2021. v. 1

GAWANDE, A. P.; KAWARE, J. P. Fuel adulteration consequences in India: a review. **Sci. Revs. Chem. Commun**, v. 3, n. 3, p. 161–171, 2013.

GOWARIKER, V. et al. **The Fertilizer Encyclopedia**. Hoboken, NJ, USA: John Wiley & Sons, Inc., 2009.

INAUDI, D.; BELLI, R.; WALDER, R. **Detection and localization of micro-leakages using distributed fiber optic sensing**. Proceedings of IPC2008. **Anais**...Calgary: 2008. Disponível em: <https://proceedings.asmedigitalcollection.asme.org>

KALLIGEROS, S. et al. **Fuel adulteration issues in Greece Energy**. [s.l: s.n.]. Disponível em: <www.elsevier.com/locate/energy>.

KORLAPATI, N. V. S. et al. **Review and analysis of pipeline leak detection methods**. **Journal of Pipeline Science and Engineering**KeAi Communications Co., , 1 dez. 2022.

LONGWELL, H. J. The Future of the Oil and Gas Industry - Past Approaches, New Challenges. **World Energy**, v. 5, n. 3, p. 100–104, 2002.

LOTFI, M.; NOORI, M. A highly-sensitive temperature sensor based on GeO2-SiO2long period fiber grating. **Physica Scripta**, v. 96, n. 1, 1 jan. 2021.

MAJHI, A. et al. The detection of kerosene as an adulterant in gasoline. **Petroleum Science and Technology**, v. 30, n. 3, p. 271–277, 14 dez. 2011.

MANCINI, L.; PAZ, M. J. Oil sector and technological development: Effects of the mandatory research and development (R&D) investment clause on oil companies in Brazil. **Resources Policy**, v. 58, p. 131–143, 1 out. 2018.

MATĚJOVSKÝ, L. et al. Study of Corrosion of Metallic Materials in Ethanol-Gasoline Blends: Application of Electrochemical Methods. **Energy and Fuels**, v. 31, n. 10, p. 10880–10889, 19 out. 2017.

MEIRELLES, A.; WEISS, S.; HERFURTH, H. **Ethanol Dehydration by Extractive Distillation J. Chem. Tech. Biotechnol**. [s.l: s.n.].

NAMBI, I. M. et al. An assessment of subsurface contamination of an urban coastal aquifer due to oil spill. **Environmental Monitoring and Assessment**, v. 189, n. 4, 1 abr. 2017.

OTTO, R. et al. Nitrogen fertilizer consumption and nitrous oxide emissions associated with ethanol production – A national-scale comparison between Brazilian sugarcane and corn in the United States. **Journal of Cleaner Production**, v. 350, 20 maio 2022.

PEIXOTO E SILVA, M. S. et al. Evaluation of Fiber Optic Raman Scattering Distributed Temperature Sensor between -196 and 400 °c. **IEEE Sensors Journal**, v. 21, n. 2, p. 1527–1533, 15 jan. 2021.

RHEIMS, J.; WRIEDT, T. Refractive-index measurements in the near-IR using an Abbe refractometer. **Meas. Sci. Technol**, v. 8, n. 6, p. 601–605, 1997.

RUAN, L. et al. Nitrogen fertilization challenges the climate benefit of cellulosic biofuels. **Environmental Research Letters**, v. 11, n. 6, 2 jun. 2016.

SABET, A. H.; AGHA, M.; HEANEY, R. Value of investment: Evidence from the oil and gas industry. **Energy Economics**, v. 70, p. 190–204, 1 fev. 2018.

SANI, E.; DELL'ORO, A. Spectral optical constants of ethanol and isopropanol from ultraviolet to far infrared. **Optical Materials**, v. 60, p. 137–141, 1 out. 2016.

SEGELSTEIN, D. J. **The Complex Refractive Index of Water**. Kansas City: University of Missouri-Kansas City, 1981.

SENOUCI, A. et al. A model for predicting failure of oil pipelines. **Structure and Infrastructure Engineering**, v. 10, n. 3, p. 375–387, mar. 2014.

SNYDER, C. S. et al. Review of greenhouse gas emissions from crop production systems and fertilizer management effects. **Agriculture, Ecosystems and Environment**, v. 133, n. 3–4, p. 247–266, out. 2009.

SRIVASTAVA, S. K.; VERMA, R.; GUPTA, B. D. Surface plasmon resonance based fiber optic sensor for the detection of low water content in ethanol. **Sensors and Actuators, B: Chemical**, v. 153, n. 1, p. 194–198, 31 mar. 2011.

TENG, C. X. et al. The influence of temperature to a refractive index sensor based on a macro-bending tapered plastic optical fiber. **Optical Fiber Technology**, v. 31, p. 32–35, 1 set. 2016.

VELLO, T. P. et al. A simple capacitive method to evaluate ethanol fuel samples. **Scientific Reports**, v. 7, 27 fev. 2017.

VEMPATAPU, B. P.; KANAUJIA, P. K. **Monitoring petroleum fuel adulteration: A review of analytical methods**. **TrAC - Trends in Analytical Chemistry,** Elsevier B.V., 1 jul. 2017.

WANG, H.; DUNCAN, I. J. Likelihood, causes, and consequences of focused leakage and rupture of U.S. natural gas transmission pipelines. **Journal of Loss Prevention in the Process Industries**, v. 30, n. 1, p. 177–187, 2014.

ZABBEY, N.; OLSSON, G. Conflicts - Oil Exploration and Water. **Global Challenges**, v. 1, n. 5, p. 1600015, ago. 2017.

ZHANG, Y.; ZHONG, X.; LI, Z. **Oil Well Real-time Monitoring With Downhole Permanent FBG Sensor Network**. [s.l: s.n.].

ZHONG, X. et al. **Distributed temperature sensing technology for oil and gas wells based on weak reflection fiber bragg grating**. 2021 3rd International Conference on Intelligent Control, Measurement and Signal Processing and Intelligent Oil Field, ICMSP 2021. **Anais**...Institute of Electrical and Electronics Engineers Inc., 23 jul. 2021.

ZHOU, X.; YU, Q.; PENG, W. **Fiber-optic Fabry–Perot pressure sensor for down-hole application**. **Optics and Lasers in Engineering,** Elsevier Ltd, , 1 out. 2019.

ZOU, C. et al. Energy revolution: From a fossil energy era to a new energy era. **Natural Gas Industry B**, v. 3, n. 1, p. 1–11, 1 jan. 2016.

APPENDIX A – LIST OF PUBLICATIONS

A.1. PEER-REVIEW PUBLICATIONS

- M. S. Peixoto e Silva, **T. H. C. de Barros**, H. P. Alves, J. F. Nascimento and J. F. Martins- Filho, "Evaluation of fiber optic Raman scattering distributed temperature sensor between–196 and 400° C". *IEEE Sensors Journal*, v. 21, n. 2, pp. 1527-1533, 2021. DOI: https://doi.org/10.1109/JSEN.2020.3016322.
- H. P. Alves, **T. H. C. de Barros**, D. L. S., Nascimento, M. S. Peixoto e Silva, J. F do Nascimento, E. Fontana, and J. F. Martins-Filho, "Influence of surface roughness on the sensitivity of a D-shaped optical fiber-based refractive index sensor". Sensors and Actuators A: Physical, v. 344, p. 113702, 2022.
  DOI: https://doi.org/10.1016/j.sna.2022.113702.

A.2. NATIONAL CONFERENCES PUBLICATIONS

- **T. H. C. de Barros**, L. S. C. Miranda, H. P. Alves, M. S. P. e Silva, and J. F. Martins-Filho, "Sensor Digital Multiponto a Fibra Óptica para Detecção de Óleo". In: 20º Simpósio Brasileiro de Micro-Ondas e Optoeletrônica. 2022.
- **T. H. C. de Barros**, J. E. S. Sousa, H. P. Alves and J. F. Martins-Filho, “Medidor de Potência Óptica para Fabricação de Perfil D em Fibra Óptica Plástica”. In: 20º Simpósio Brasileiro de Micro-Ondas e Optoeletrônica. 2022.
- H. P. Alves, **T. H. C. de Barros**, A. A. D. da Silva, L. D. Coelho and J. F. Martins-Filho, “Modulador Eletro-Óptico Integrado à Fibra de Perfil D”. In: 20º Simpósio Brasileiro de Micro-Ondas e Optoeletrônica. 2022.

A.3. INTERNATIONAL CONFERENCES PUBLICATION

- **T. H. C. de Barros**, J. E. S. Sousa, H. P. Alves and J. F. Martins-Filho, “D-Shaped Plastic Optical Fibers: Fabrication and Characterization as Refractive Index Sensor”. In 2021 SBMO/IEEE MTT-S International Microwave and Optoelectronics Conference (IMOC). IEEE, p.1-3, 2021.

- **T. H. C. de Barros**, H. P. Alves, R. E. de Araujo and J. F. Martins-Filho, “Computational Modeling of D-shaped Optical Fiber Nitrate and Sulfate Sensor”. In 2022 SBFoton International Optics and Photonics Conference (SBFoton IOPC). IEEE, p. 1-4, 2022.
- **T. H. C. de Barros**, J. E. S. Sousa, H. P. Alves and J. F. Martins-Filho, “D-shaped optical fiber refractive index sensor for application in fuel oil mixtures and leakage detection”. In Proceedings of the Rio Oil & Gas Expo and Conference. IBP, p. 1-11, 2022.
- **T. H. C. de Barros**, H. P. Alves, H. J. B. de Oliveira and J. F. Martins-Filho, “D-shaped Plastic Optical Fiber Sensor for Detection of Ethanol Fuel Adulteration”. In 2023 SBFoton International Optics and Photonics Conference (SBFoton IOPC). IEEE, p. 1-2, 2023.
- H. J. B. de Oliveira, **T. H. C. de Barros**, A. A. D. da Silva, J. F. do Nascimento and J. F. Martins-Filho, “Refractive Index Sensor based on Hetero-core Fiber Interrogated by a Laser/fotodetector at 1550 nm”. In 2023 SBFoton International Optics and Photonics Conference (SBFoton IOPC). IEEE, p. 1-2, 2023.
- **T. H. C. de Barros**, L. S. C. de Miranda, H. P. Alves and J. F. Martins-Filho, “Multipoint sensor based on D-shaped optical fiber for detection of leaks in pipelines”. In Proceedings of the Rio Pipeline Conference & Exhibition 2023. IBP, p. 1-11, 2023.
- L. S. C. de Miranda, **T. H. C. de Barros**, H. P. Alves and J. F. Martins-Filho, “Computational Modeling of D-shaped Optical Fiber Corrosion Sensor for Oil Environment”. In Proceedings of the Rio Pipeline Conference & Exhibition 2023. IBP, p. 1-8, 2023.
- **T. H. C. de Barros**, L. S. C. Miranda, H. P. Alves and J. F. Martins-Filho, “Diesel Adulteration Sensor Based on D-Shaped Optical Fiber”. In 2023 SBMO/IEEE MTT-S International Microwave and Optoelectronics Conference (IMOC). IEEE, p.1-3, 2023.